BSGF - Earth Sciences Bulletin 2021, 192, 3
© C. Montmartin *et al.*, Published by EDP Sciences 2021
https://doi.org/10.1051/bsgf/2020043

BSGF
Earth Sciences Bulletin
Available online at:
www.bsgf.fr

Paleotemperature investigation of the Variscan southern external domain: the case of the Montagne Noire (France)

Clément Montmartin*, Michel Faure and Hugues Raimbourg

Institut des Sciences de la Terre d'Orléans (ISTO), UMR 7327, Université d'Orléans-CNRS-BRGM, Campus Géosciences, 1A Rue de la Férollerie, 45071 Orléans Cedex 2, France

Received: 26 June 2020 / Accepted: 8 October 2020

Abstract – The Montagne Noire located in the southern part of the French Massif Central represents the northern part of the South-Variscan Foreland. It is subdivided into three parts. The granite-migmatite Axial Zone dome is surrounded by non- or weakly metamorphosed Paleozoic sedimentary series. Both northern and southern flanks of the Montagne Noire dome are deformed by km-scale, south to southeast facing recumbent folds and thrusts sheets. The Raman Spectroscopy of Carbonaceous Material (RSCM) method, carried out in the low-grade metamorphic rocks of the southern flank of the Montagne Noire, yielded temperatures comprised between 400 °C near the dome, and 230 °C in the southern domain. Three Raman geothermometers were used to cover this temperature range. RSCM temperatures comply qualitatively with previous estimates based on illite crystallinity, conodont color alteration, and fluid inclusions carried out in the same area, which document a metamorphic temperature increase towards the dome. The isotherms cut across the different nappe contacts and are oriented parallel to the southern margin of the Axial Zone. This temperature distribution supports the idea that the thermal structure was acquired during the Axial Zone dome emplacement. The thermal structure acquired during the recumbent folds emplacement and burial of the sedimentary series is totally overprinted by the doming event. In addition, in a domain relatively remote from the Axial Zone dome, the RSCM measurements yielded significantly higher temperatures than illite crystallinity. This discrepancy points to a higher sensitivity of RSCM to short-lived thermal events than illite crystallinity, possibly because of more efficient kinetics of the carbonization reaction. On the other hand, high RSCM temperatures analysed far from the Axial Zone, between 300 °C and 360 °C could be explained by the presence of granitic plutons under the foreland basin.

Keywords: Raman Spectroscopy of Carbonaceous Material (RSCM) / Granite-migmatite dome / Montagne Noire / Variscan orogen / French Massif Central / Recumbent folds

Résumé – Étude de paléotempérature dans le domaine méridional externe varisque: le cas de la Montagne Noire (France). La Montagne Noire, située dans la partie sud du Massif Central français, représente la partie nord de l'avant-pays varisque. La zone est divisée en trois parties. Le dôme granite-migmatite de la zone axiale est entouré de séries sédimentaires paléozoïques pas ou faiblement métamorphisées. Les flancs nord et sud du dôme de la Montagne Noire sont déformés par des plis d'échelle kilométrique, déversés vers le sud sud-est. La méthode de spectrométrie Raman de la matière carbonée (RSCM), réalisée dans les roches de bas grade métamorphique du flanc sud de la Montagne Noire, a donné des températures comprises entre 400 °C près du dôme et 230 °C dans le domaine sud. Trois géothermomètres Raman ont été utilisés pour couvrir cette gamme de température. Ces températures RSCM sont qualitativement conformes aux estimations précédentes basées sur la cristallinité de l'illite, la couleur d'altération des conodontes et les inclusions fluides effectuées dans la même zone, qui démontrent une augmentation de la température vers le dôme. Les isothermes traversent les différents contacts de nappe et sont orientées parallèlement à la marge sud de la zone axiale. Cette distribution de température suggère que la structure thermique a été acquise lors de la mise en place du dôme de la zone axiale. La structure thermique acquise lors de la mise en place des plis couchés et de l'enfouissement des séries sédimentaires est ainsi totalement effacé par le dôme. De plus, dans un domaine relativement éloigné du dôme de la zone axiale, les mesures RSCM ont donné des températures significativement plus élevées que la cristallinité de

*Corresponding author: clement.montmartin@univ-orleans.fr

l'illite. Cette divergence indique une sensibilité plus élevée du RSCM face à la cristallinité de l'illite aux événements thermiques de courte durée, probablement en raison d'une cinétique plus efficace de la réaction de carbonisation/graphitisation. D'autre part, de fortes températures RSCM analysées loin de la Zone Axiale, entre 300 °C et 360 °C, pourraient être expliquées par la présence de plutons granitiques sous le bassin d'avant-pays.

Mots clés : Spectrométrie Raman de la Matière Carbonée (RSCM) / Dôme granite-migmatite / Montagne Noire / Orogenèse Varisque / Massif Central Français / Plis couchés

1 Introduction

The knowledge of quantitative constraints, such as pressure, temperature, duration of heating, strain, strain rate, exhumation rate, and uplift rate, is essential to understand the formation and evolution of a mountain belt. In recent years, many studies (*e.g.* Beyssac *et al.*, 2002; Gerya and Stöckhert, 2002) dealt with these issues thanks to significant advances in petrology and geochronology. In the inner domain of an orogen, temperature and pressure conditions experienced by metamorphic rocks can be approached by petrological investigations based on mineral parageneses. On the contrary, in the outer domain, where the deformation and associated metamorphism are usually less developed than in the inner domain, the evaluation of the thermo-barometric conditions is difficult, since the size of syn-tectonic metamorphic minerals is generally small and conditions of thermodynamic equilibria are often not achieved (Frey, 1987; Merriman and Frey, 1999; Merriman and Peacor, 1999). The measurement of low temperature or low pressure values is therefore delicate, and often bears a large error. However, several methods have been developed to overcome this problem and to reach a quantitative knowledge of the conditions of low-grade metamorphism, including illite crystallinity, conodont alteration colour, calcite-dolomite thermo-barometer (*e.g.* Kübler, 1968; Dunoyer de Segonzac *et al.*, 1968; Epstein *et al.*, 1977; Frey, 1987). More recently, the Raman Spectroscopy of Carbonaceous Material (RSCM) method based on carbonaceous material crystallinity has been developed for the temperature range 330–650 °C (Beyssac *et al.*, 2002). Its applicability has been further extended towards low temperatures (Rahl *et al.*, 2005; Lahfid *et al.*, 2010; Kouketsu *et al.*, 2014), using different calibrations of the Raman spectra based on other geothermometers, such as vitrinite reflectance, fluid inclusions microthermometry or illite crystallinity (Rahn *et al.*, 1995, Hara *et al.*, 2013) or indirect data on temperature provided by fission-tracks and U-Th/He method (Rahl *et al.*, 2005).

The applicability of the RSCM method is *a priori* restricted to the conditions of its calibration. In all the different studies that focused on RSCM at low temperature, the case studies were chosen in subduction or collision settings such as Sanbagawa Belt in Japan (Kouketsu *et al.*, 2014) and the Glarus Alps in Switzerland (Lahfid *et al.*, 2010), providing examples of metamorphic gradients. Therefore, in these cases, the thermal imprint on the rocks is related to burial then exhumation within a subduction zone or a collision belt, *i.e.* the thermal event lasts for at least one or several million years. Heating by a magmatic intrusion is potentially much shorter-lived and the inter-compatibility of the different geothermometers in such a case is not guaranteed (Velde and Lanson, 1993).

When compared to other geothermometers, the biases linked to the kinetics of the thermal recording by the carbonaceous material with respect to other mineral reactions should be considered (Velde and Lanson, 1993; Mullis *et al.*, 2017). It appears that duration of heating heavily impacts maturity processes and is a key parameter that controls the measured temperature (Wada *et al.*, 1994; Mählmann, 2001; Le Bayon *et al.*, 2011; Mori *et al.*, 2017). Moreover, the geothermometers based on carbonaceous material differ from fluid inclusion or metamorphic mineral ones mostly because no water is needed for the maturation of carbonaceous material (Velde and Lanson, 1993; Le Bayon *et al.*, 2011). Thus, even if the whole rock experienced the same thermal history, disparities might be observed between the different methods.

Further complexity arises when dealing with multi-metamorphic events, as in the case of post-orogenic, large-scale heating and pluton emplacement postdating collisional metamorphism, for instance in the Jebilet Massif in Moroccan Variscan Belt (Delchini *et al.*, 2016). A contact metamorphism linked to a magmatic intrusion may overprint the crystallinity of carbonaceous material inherited from earlier stages, as it has already been documented in several studies. For instance, Mori *et al.* (2017), measured temperatures imposed by thin (50 m) magmatic bodies such as the Great Whin Sill in the UK, overprinting the regional low-grade metamorphism (< 300 °C). On a larger scale, Aoya *et al.* (2010) focussed on contact metamorphic aureoles around granitic plutons in Japan within two poorly metamorphosed accretionary complexes (< 400 °C). Hilchie and Jamieson (2014) have studied the South Mountain Batholith intrusion thermicity of Nova Scotia emplaced under a regional greenschist facies metamorphism. In each case, RSCM temperatures decrease with the distance to the intrusive bodies. Finally, shear heating between structural units could also influence the organic matter organization (*e.g.* Mori *et al.*, 2015). The interpretation of RSCM data in domains with a poly-stage metamorphic evolution is therefore often ambiguous, as the RSCM measurements combine the contribution of regional syn-tectonic metamorphism coeval with crustal thickening due to nappe stacking and the later thermal overprint related to a magmatic event.

The present study aims to decipher the thermal evolution recorded in a cold foreland domain of a collisional orogen overprinted by a hot metamorphic dome (*e.g.* Gèze, 1949; Schuiling, 1960; Demange, 1982; Echtler and Malavieille, 1990; Soula *et al.*, 2001; Alabouvette *et al.*, 2003; Franke *et al.*, 2011). The study area is located in the southern outer zone of the Variscan belt, in the Montagne Noire of the French Massif Central (Fig. 1). The bulk paleotemperature field is derived from 72 RSCM measurements of graphite crystallinity on

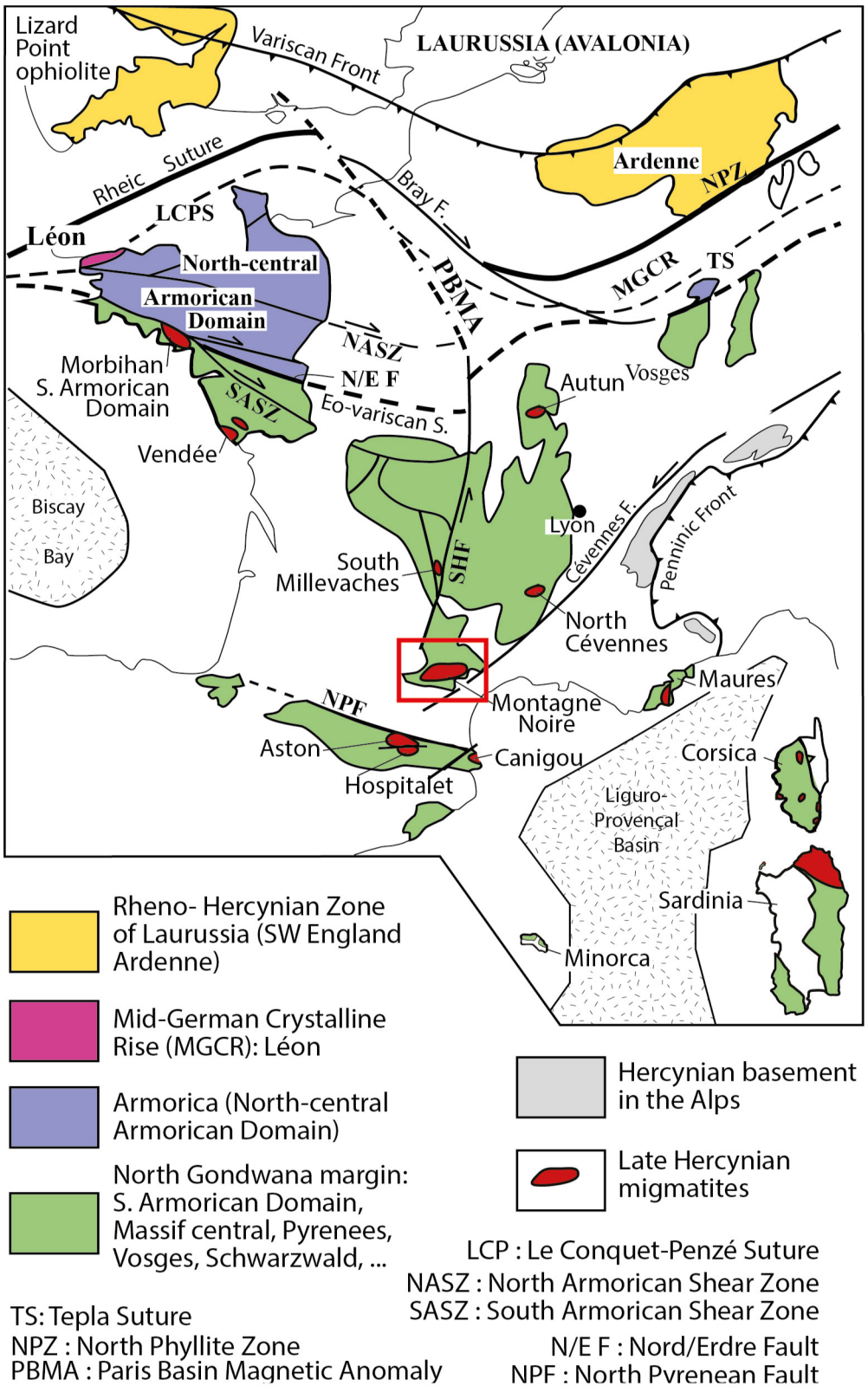

Fig. 1. Variscan massifs map with location of the Visean-Serpukhovian migmatites. The red rectangle represents the study area (modified from Faure *et al.*, 2010).

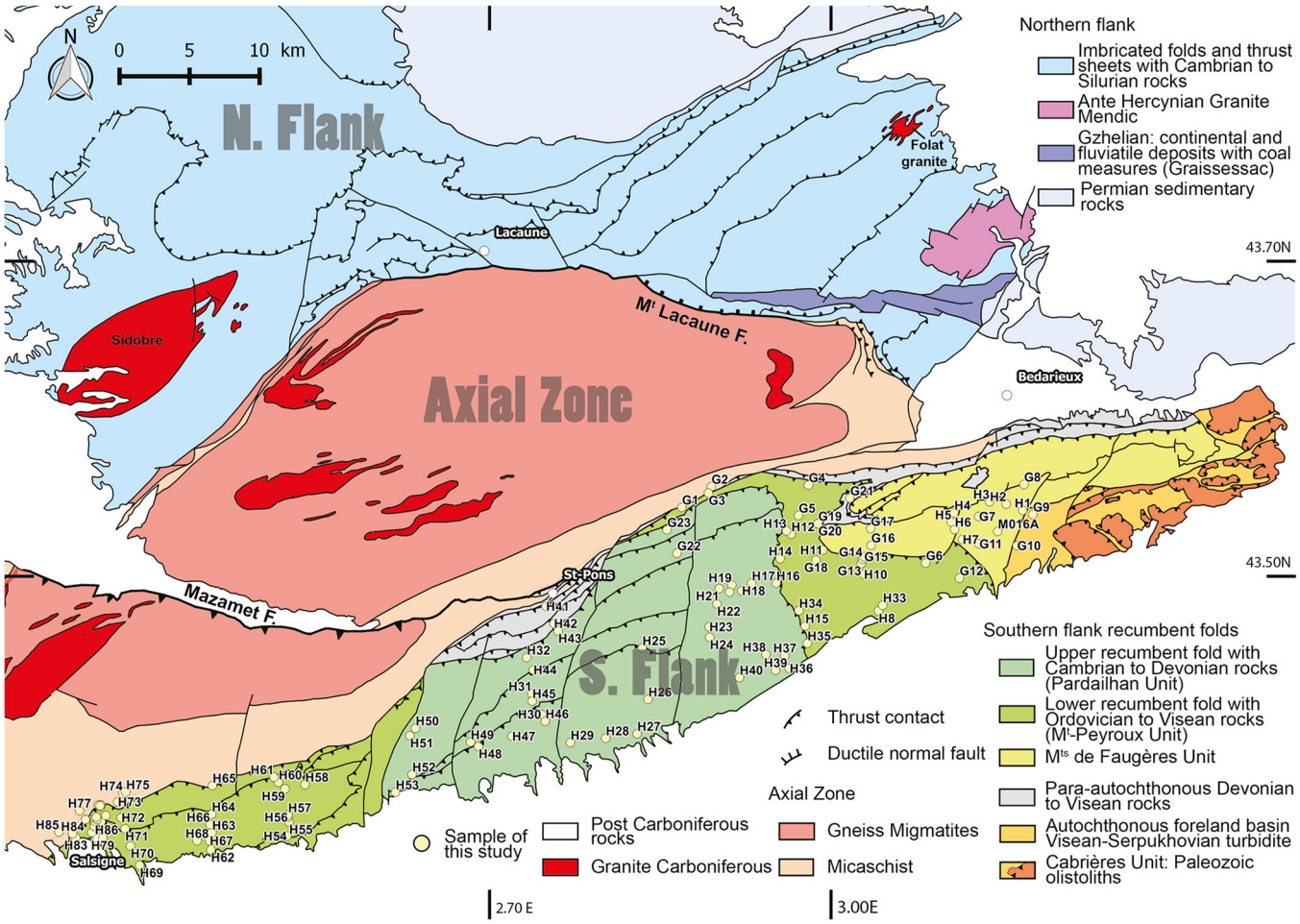

Fig. 2. Simplified structural map of the Montagne Noire showing the granite-migmatite dome of the Axial Zone, and the sedimentary northern and southern flanks (modified from Gèze, 1949; Arthaud, 1970; Faure *et al.*, 2010). The recumbent folding in the south area is coeval with the sedimentation in the Visean-Serpukhovian basin. The stratigraphy presents a reverse order in most part of these series. The figure was made from the vectorised map 250 000 of Montpellier by the BRGM (Berger *et al.*, 2001).

weakly deformed silts and pelites from Paleozoic formations that constitute the southern Variscan fold-and-thrust belt of the Massif Central. These new results are discussed in the tectonic framework of this segment of the Variscan orogen.

2 Geological background

The Variscan belt develops from South Spain to Poland. The French Massif Central is a stack of nappes formed through a long and complex polyorogenic evolution (for details see Faure *et al.*, 2005, 2009, 2017). The SE part of the Massif exposes a succession of thrusts and nappes formed from Visean to Bashkirian during the late collisional intracontinental evolution (the D3 event of Faure *et al.*, 2009). In the Montagne Noire area, the southernmost part of Massif Central, weakly metamorphosed sedimentary series develop in a southeast-verging fold-and-thrust belt (Fig. 1). There, kilometre-scale recumbent folds affect the entire sedimentary series, including the Visean-Serpukhovian flysch. Over the whole belt, the crustal thickening resulting from the successive emplacement from North to South of large-scale nappes (UGU, LGU, PAU), was followed by pervasive melting affecting the tectonic pile. Middle to Late Carboniferous migmatites and granites are widespread in the Massif Central (Fig. 1).

3 The outer Variscan domain in the Montagne Noire

3.1 General structure

The Montagne Noire is subdivided into southern and northern flanks separated by the Axial Zone (*e.g.* Gèze, 1949; Arthaud, 1970; Fig. 2). The former two zones consist of Cambrian, Ordovician, Devonian and Carboniferous sedimentary rocks folded and thrust to the south from the Visean to the Serpukhovian. The Axial Zone is a granite-migmatite dome emplaced within the folded series. Paleozoic formations are well exposed in the Montagne Noire southern flank (Fig. 3). Detailed lithological descriptions are available in Gèze (1949); Feist and Galtier (1985); Álvaro *et al.* (1998); Vizcaïno and Álvaro (2001) and Alabouvette *et al.* (2003). The Visean-Serpukhovian series, well exposed on the southern flank, consists of syn-tectonic gravity flow deposits such as greywacke turbidites and olistostromes, which recycle

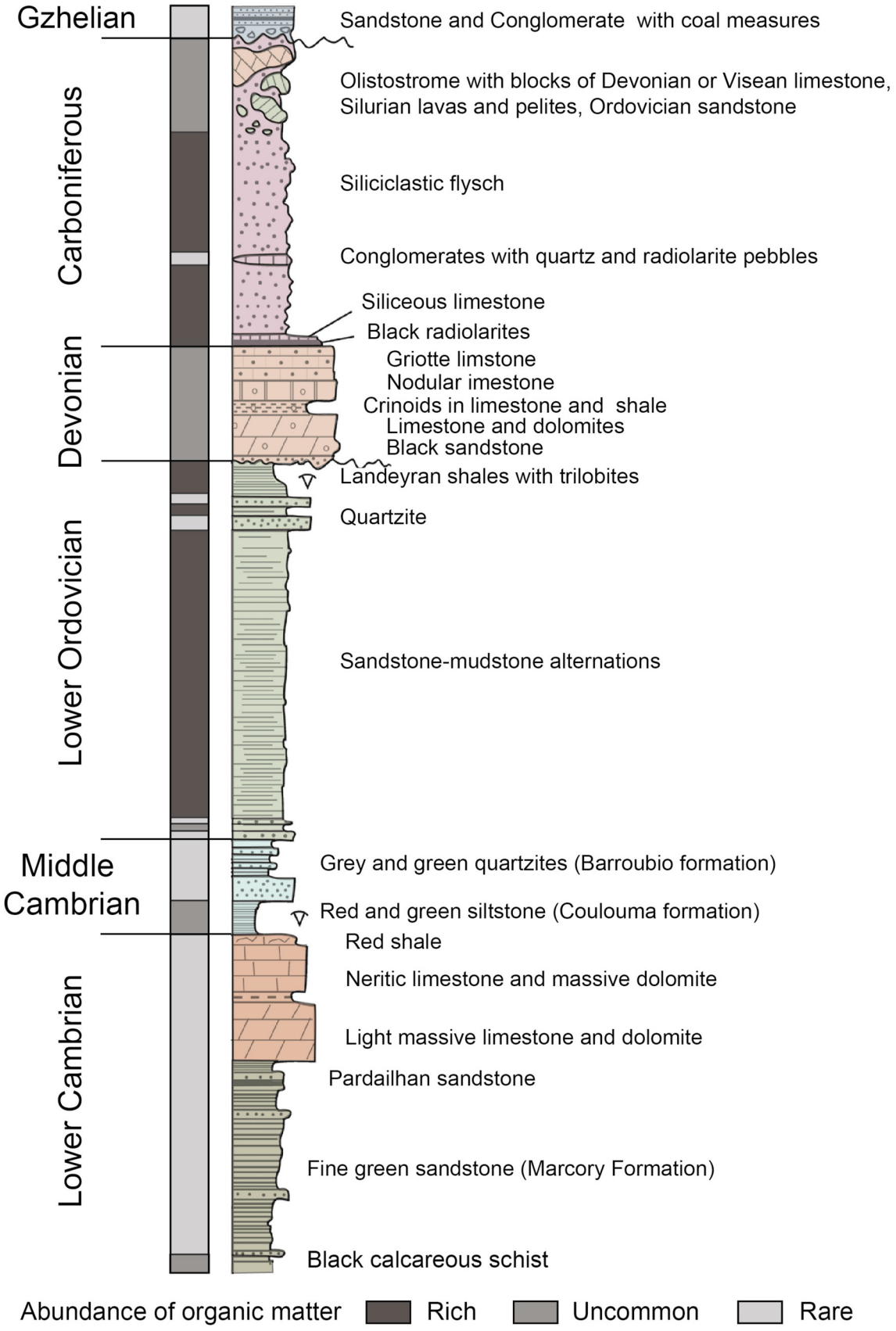

Fig. 3. Paleozoic stratigraphic log, with the abundance in organic matter shown on the left column (modified from Arthaud, 1970; Engel *et al.*, 1980-1981; Álvaro and Vizcaïno, 1998; and Vizcaïno and Álvaro, 2001).

pre-Visean sedimentary rocks of the advancing nappe pile (Engel *et al.*, 1978, 1980-1981; Feist and Galtier, 1985; Poty *et al.*, 2002; Vachard and Aretz, 2004; Cózar *et al.*, 2017; Vachard *et al.*, 2017). During the Carboniferous, the progressive deepening of the sedimentary basin argues for a foreland trough, filled by syntectonic deposits, and coeval with the formation of recumbent folds. The entire Paleozoic series has been deformed into several km-scale, southeast-verging, thrust sheets and recumbent folds (Arthaud 1970; Echtler and Malavieille, 1990).

3.2 Tectonic subdivisions

3.2.1 The Southern Flank

The upper recumbent fold, or Pardailhan unit, is the highest tectonic unit of the southern flank of the Montagne Noire. It is composed of Cambrian to Devonian sedimentary rocks with an inverted stratigraphic order, *i.e.* the geometrically upper part consists of Early Cambrian sandstone, and the lower part is formed by Devonian limestone boudins that delimit the basal shear zone separating the upper recumbent fold from the lower one. From north to south, perpendicularly to the fold axes, the inverted limb of the Pardailhan recumbent fold develops along 12 km. These inverted sedimentary series are subdivided into three km-scale recumbent anticlines overturned to the south (Gèze, 1949; Arthaud, 1970; Alabouvette *et al.*, 1982, 2003).

Structurally below the upper recumbent fold, the lower one, also named Mt-Peyroux unit, can be observed both in the eastern and western sides of the upper recumbent fold (Fig. 2). The western part of the lower recumbent fold is called the Minervois unit. The highest part of this recumbent fold is occupied by Ordovician flysch while Visean turbidites crop out in the lower part, indicating a stratigraphic inversion. NE-SW upright antiforms and synforms deform the inverted series of the entire nappe stack. The poorly exposed contact between the lower recumbent fold and the foreland basin led to controversial interpretations. According to Arthaud (1970), and Alabouvette *et al.* (1982, 2003) the inverted limb is in contact with Visean-Serpukhovian turbidites. However, according to (Engel *et al.*, 1978, 1980-1981), the flysch sequence is part of the lower recumbent (Mt. Peyroux) fold. The normal and inverted limbs of that fold nappe are connected by a D1 fold hinge. Whatever the structural interpretation, this does not change the RSCM results presented below, and their interpretations. The presence of Paleozoic olistoliths in the Visean-Serpukhovian turbidites basin in which the recumbent folds are emplaced documents the syn-sedimentary character of this event. It provides an important time constraint for the tectonic evolution of the southern flank: the nappe thrusting is contemporary or older than 318 Ma (Engel *et al.*, 1978, 1980-1981; Alabouvette *et al.*, 1982, 2003; Vachard *et al.*, 2017).

Below the eastern part of the lower (Mt Peyroux) recumbent fold, characterized by overturned Ordovician to Early Carboniferous series, the Mts de Faugères unit consists of Devonian and Early Carboniferous sedimentary rocks deformed by southeast-verging recumbent folds. The Para-autochthon unit is composed of Devonian to Middle Carboniferous sedimentary rocks exposed in the normal stratigraphic order. This domain is observed between the lower recumbent fold and the Axial Zone metamorphic rocks. Close to the Axial Zone, for instance near Saint-Pons (Fig. 2), the Para-autochthonous unit consists of Devonian marbles and micaschists (Engel *et al.*, 1980-1981; Feist and Galtier, 1985; Poty *et al.*, 2002; Vachard and Aretz, 2004; Cózar *et al.*, 2017; Vachard *et al.*, 2017).

The autochthonous turbiditic basin represents the foreland basin into which the Mt-Peyroux and Mts-de-Faugères recumbent folds were emplaced. The basin substratum is unknown but might probably be similar to that observed in the northern para-autochthonous unit. To the west, the basin underlies the stack of recumbent folds, and to the south, it is hidden below the Cenozoic formations.

3.2.2 The Axial Zone

The Axial Zone is composed of orthogneiss, paragneiss, amphibolite, micaschist, and rare marble that experienced a partial melting giving rise to migmatites and granites. The Axial Zone presents a dome architecture of about 90 km long, and 20 km wide, with a N70E long axis (Gèze, 1949; Faure and Cottereau, 1988; Echtler and Malavieille, 1990; Matte *et al.*, 1998; Van Den Driessche and Brun, 1992; Demange, 1993; Alabouvette *et al.*, 2003). The Eocene Pyrenean Mazamet fault divides the western part of the dome in two parts, the Agout and Nore massifs in the North and South, respectively. The orthogneiss yields zircon U-Pb Ordovician to Devonian ages at 472 ± 2.8 Ma, 456 ± 3 Ma, 450 ± 6 Ma, 455 ± 2 Ma, and 416 ± 5 Ma interpreted as those of the granite protolith (Roger *et al.*, 2004; Cocherie *et al.*, 2005; Franke *et al.*, 2011; Pitra *et al.*, 2012; Trap *et al.*, 2017). The country rocks protoliths of these orthogneiss are interpreted as Neoproterozoic to Cambrian or Ordovician (Alabouvette *et al.*, 2003). Several geochronological ages on the migmatite and anatectic granites range between 333 Ma and 294 Ma (Hamet and Allègre, 1976; Faure *et al.*, 2010; Franke *et al.*, 2011; Poilvet *et al.*, 2011; Roger *et al.*, 2015; Trap *et al.*, 2017) with pegmatite until 282 Ma (Doublier *et al.*, 2015). The abundance of granitoids and migmatite argue for a widespread thermal event. The Axial Zone experienced two metamorphic and tectonic events. The early one is recorded only in rare mafic eclogitic restites enclosed in the migmatite. Though zircon in eclogite yields a ca. 315 Ma age (Faure *et al.*, 2014; Whitney *et al.*, 2015), this can hardly be interpreted as the age of the high pressure event since the enclosing migmatite yields ages older than the eclogite blocks. A hydrothermal event might be responsible for zircon recrystallization. The second, and main one is coeval with the dome formation (Schuiling, 1960; Bard and Rambeloson, 1973; Thompson and Bard, 1982; Soula *et al.*, 2001; Faure *et al.*, 2014; Fréville *et al.*, 2016; Trap *et al.*, 2017).

The metasedimentary rocks that form the outer envelope of the granite-migmatite dome underwent a pervasive high temperature/medium pressure (HT/MP) metamorphism coeval with the dome formation (Soula *et al.*, 2001; Faure *et al.*, 2014; Fréville *et al.*, 2016). From South to North, chlorite, biotite, garnet, andalousite, staurolite, and sillimanite isograds appear successively. As already pointed out, chlorite, biotite, and muscovite belonging to the low temperature part of the HT/MP metamorphism develops in the various lithotectonic units close to the Axial Zone, such as the para-autochthonous, Mts-de-

Faugères, Mt-Peyroux and Pardailhan units (Arthaud, 1970; Franke *et al.*, 2011; Fréville *et al.*, 2016). The Axial Zone HT/MP metamorphism started after the emplacement of the thrusts and recumbent folds but continued still afterwards into the Permian (Alabouvette *et al.*, 2003; Franke *et al.*, 2011; Pitra *et al.*, 2012).

3.2.3 The Northern Flank

The Montagne Noire northern flank is composed of Late Neoproterozoic (Ediacaran) to Silurian sedimentary formations subdivided into several south-directed folds and thrusts considered as equivalent to those of the southern flank. The deformation age is estimated of Visean age (342–333 Ma; Gèze, 1949; Alabouvette *et al.*, 2003; Doublier *et al.*, 2006). The southern part of the northern flank, east and SW of the Lacaune fault (Fig. 2), exposes biotite, garnet, andalousite micaschists comparable to the metapelites of the southern envelope of the Axial Zone (Demange, 1982). This metamorphism that superimposes to the fold-and thrust structure was coeval with the HT/MP event related to the Axial Zone doming (Doublier *et al.*, 2006). The contact between the northern flank and Axial Zone is the Mts-de-Lacaune NE-dipping ductile normal fault that accommodated the dome emplacement (Van Den Driessche and Brun, 1989). Furthermore, a brittle normal fault controlled the opening of the Late Carboniferous (Gzhelian) Graissessac coal basin. In the following, the northern flank will not be considered.

3.3 The tectonic outline of the southern flank

The structural analysis of the Montagne Noire southern flank revealed two main tectonic events (Arthaud, 1970). The first deformation stage corresponds to the emplacement of the south verging recumbent folds (F1) and thrusts. The bedding and cleavage relationships demonstrate the south to southeastward vergence of the F1 folds (Arthaud, 1970; Fig. 4a). A recent study proposes a nappe thrusting towards the northeast (Chardon *et al.*, 2020). Whatever the tectonic interpretation, in spite of 15 km of subhorizontal displacement, and the ca 1.5 km overload due to the stratigraphic inversion, the Paleozoic series poorly exhibit a ductile syn-metamorphic deformation. A slaty cleavage is only visible in the hinges of F1 folds (Arthaud, 1970). The metamorphic grade reached by the upside down Paleozoic series in the Upper (Pardailhan) and Lower (Mt-Peyroux) recumbent folds is below the biotite grade, which firstly appear near the dome, in the para-autochthonous unit.

The second deformation event is an upright folding phase (F2). Field observations document the refolding of the F1 recumbent folds by the F2 upright ones with NE-SW striking axes (Arthaud, 1970; Alabouvette *et al.*, 2003). Close to the Axial Zone, a subvertical axial planar cleavage develops in the F2 folds, whereas away from the Axial Zone dome, the F2 folds are rather open and devoid of cleavage (Fig. 4b). The F2 upright folding corresponds to a NW-SE shortening that formed large- scale antiforms and synforms including the Axial Zone dome. A N70 mineral and crenulation lineation appears in the Carboniferous formation at about 5 km south of the dome and northward (Harris *et al.*, 1983). Sericite is also

Fig. 4. Pictures showing the two main deformation phases in the Montagne Noire southern flank. (a). Steep inverted limb of a S-verging fold coeval with the formation of the km-scale recumbent folds (F1), near Ferrals-les-Montagnes. Sample H52 was picked up for RSCM study. (b). Upright fold with axial planar cleavage (S2) coeval with the Axial Zone doming (F2) and location of the sample H41, close to St-Pons. The folded layers are S0-S1 surface where (S1) is coeval with recumbent folding (F1).

recognized north of this point (close to sample H11 – Fig. 2). However, Franke *et al.* (2011) interpreted this lineation as an extension direction linked to the pull apart emplacement of the Axial Zone. Anyhow, these metamorphic and structural features argue for a syntectonic metamorphism linked to the doming (Soula *et al.*, 2001; Franke *et al.*, 2011).

4 The RSCM method

The Raman Spectroscopy of Carbonaceous Material (RSCM) method was carried out to estimate the paleotemperature field of the low grade, weakly deformed, sedimentary rocks of the southern flank of the Montagne Noire. The method is based on the irreversible transformation of carbonaceous matter towards graphite structure, using empirical correlations to correlate Raman spectra of carbonaceous matter into maximum temperature of heating, in the range 200–650 °C (Beyssac *et al.*, 2002, Lahfid *et al.*, 2010).

4.1 Analytical settings

The Raman measurements were carried out on a Renishaw inVia reflex system belonging to the ISTO-BRGM analytic platform. The Wire 3.4 software was used for the data acquisition. The argon-ion laser source excitation of 514.5 nm was set at a power of about 5% of its capacity (2.5 mW). The monochromatic ray was coupled to a reflection microscope with an x100 objective. Before each series of measurement, the spectrometer was calibrated using an internal silica standard for the wavenumber (520.4 cm^{-1}) and the signal intensity

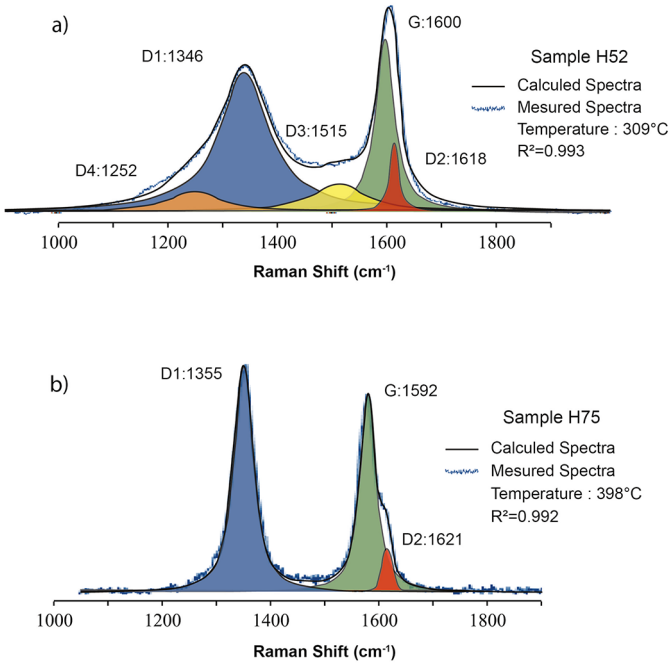

Fig. 5. Peakfitting of samples H52 (a), and H75 (b) by low temperature (Lahfid *et al.*, 2010) and high temperature method (Beyssac *et al.*, 2002), respectively.

(at least 30 000 counts per second). Fifteen carbonaceous matter spectra were systematically acquired for each sample within the thin section in order to obtain a representative and reliable temperature. Only organic particles located below transparent quartz, a few μm under the thin section surface, were analysed, to avoid any mechanical damaging of their crystalline structure due to thin section preparation and polishing. The acquisition duration was set to at least 60 s and adapted depending on the quality of the spectrum.

4.2 RSCM data processing

Several empirical calibrations were proposed to correlate the carbonaceous matter Raman spectra to temperature (Beyssac *et al.*, 2002; Rahl *et al.*, 2005; Aoya *et al.*, 2010; Lahfid *et al.*, 2010; Kouketsu *et al.*, 2014). Carbonaceous matter presents characteristic Raman bands in the wavenumber range between 1100–1800 cm^{-1} and 2500–3100 cm^{-1}. The first order region of the carbonaceous matter spectrum for 1100–1800 cm^{-1} provided the data of this study.

Depending on its crystallinity (hence on the temperature experienced), carbonaceous matter presents a variable number of Raman peaks, which can be used to discriminate between the different calibration methods. Since the sedimentary rocks of the Montagne Noire southern flank are weakly to unmetamorphosed, most of the Raman spectra were processed with the Lahfid *et al.* (2010) method. Accordingly, each spectrum was decomposed into five bands (Lorentzian functions), with a well-constrained position: G (1590 cm^{-1}) D1 (1350 cm^{-1}), D2 (1620 cm^{-1}), D3 (1515 cm^{-1}) and D4 (1250 cm^{-1}) (Lahfid *et al.*, 2010; Sadezky *et al.*, 2005). From this decomposition, the RSCM temperature was computed using the formula proposed by Lahfid *et al.* (2010) which is valid between 200 °C and 320 °C, with an accuracy of ± 30 °C (Fig. 5a):

$$T°C = \frac{RA1 - 0.3758}{0.0008} \text{ with } RA1 = \frac{D1+D4}{D1+D2+D3+D4+G}.$$

Samples with higher crystallinity have fewer Raman peaks and were processed accordingly using the method proposed by Beyssac *et al.* (2002) that allows an estimation of temperature in the range between 330 up to 650 °C, with a ± 50 °C uncertainties (Fig. 5b):

$$T°C = (-445 * R2 + 641) \text{ with } R2 = \frac{D1}{D1+D2+G}.$$

Considering the low metamorphic grade of the analysed samples, only the low range of this method was used (< 400 °C). Since the Beyssac *et al.* (2002) and Lahfid *et al.* (2010) methods do not exactly overlap with each another; we also used a third thermometer (Kouketsu *et al.*, 2014). This method does not correspond to peaks area ratios but focuses on the peak full width at half maximal (FWHM) of the D1 and D2 band. Because of the difficulty to distinguish the D2 band from the G band, only the formula about the former band was retained. According to this method, the temperature is derived from Raman peaks as:

$$T°C = -2.15 * (FWHM - D1) + 478.$$

The Kouketsu *et al.* (2014) method leads to temperatures comprised between 150 and 400 °C with a ± 30 °C uncertainty.

4.3 Uncertainty in RSCM temperatures

The different RSCM methods are calibrated against several geothermometers. The higher range temperatures method proposed by Beyssac *et al.* (2002) is mostly based on mineral assemblages. However, vitrinite reflectance, illite crystallinity, chlorite geothermometers were compared with RSCM spectra both in Kouketsu *et al.* (2014) and Lahfid *et al.* (2010) studies. Furthermore, thermal modelling, garnet-chlorite geothermometers were also used for calibration in Kouketsu *et al.* (2014) while Lahfid *et al.* (2010) used calcite-dolomite thermometry, quartz-chlorite isotopic thermometry and fluid inclusion. These calibrations were carried out on domains that were affected by a single metamorphic event.

The maximum error (1σ) on R2 ratio obtained by Beyssac *et al.* (2002) is ± 0.08 corresponding to a ± 36 °C intra-sample variability. Adding the uncertainty linked to the calibration of RSCM with reference temperatures, the authors considered that the uncertainty on the estimation of temperature was about ± 50 °C.

In the low temperature range, Lahfid *et al.* (2010) method uses the ratio of Raman peak spectra area, while Kouketsu *et al.* (2014) method uses the width of the peaks, to derive the paleotemperature. Kouketsu *et al.* (2014) estimated that the difference in estimated temperature due to the use of the two different methods is of the order of 50 °C.

4.4 RSCM acquisition

The temperatures derived from the RSCM method were obtained with a minimum of 10 to 15 spectra for each sample in order to ensure their validity. Some of the grains of carbonaceous matter present within a sediment might originate from the erosion of a sediment that has already been affected

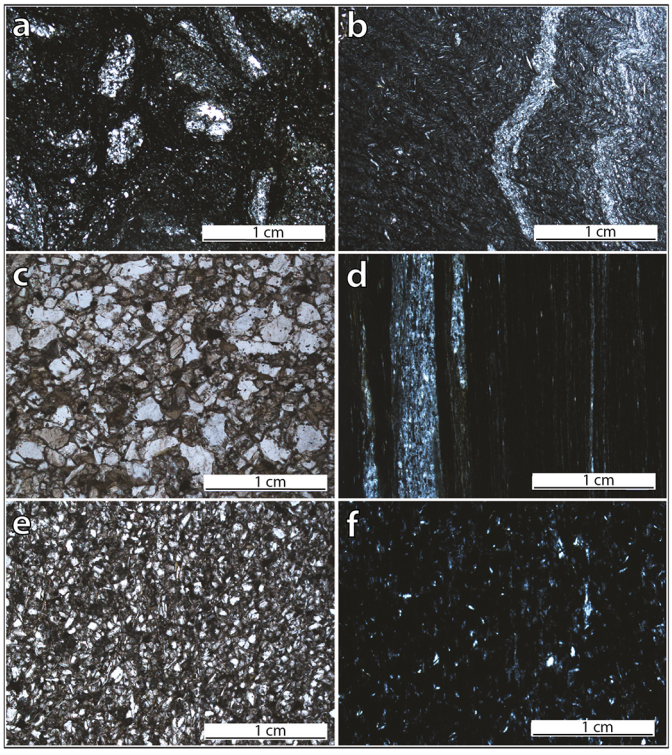

Fig. 6. Thin sections observed with optical microscope in polarized non-analysed light showing the lithology diversity, (a). Mudstone in the Visean Turbidite (sample G8), (b). Siltstone in the Early Ordovician rocks (sample G1), (c). Early Cambrian green sandstone (Marcory formation, sample H32), (d). Mudstone in the Early Ordovician rocks (sample G2), (e). Middle Cambrian fine-grained sandstone (sample H22), (f). Early Ordovician mudstone (sample G3).

by a prior metamorphic event. Since the organic matter only records the highest temperature, these inherited grains might yield higher conditions of temperature than their host sediments, if they come from higher-grade material. This case is often suspected when a few CM grains give much higher temperatures than most grains in a sample. In such a case, we disregarded the few anomalous grains and estimated the temperature from the statistical distribution concentrating most of the grains (Beyssac *et al.*, 2002).

The 122 samples analysed cover the major part of the Montagne Noire southern flank in order to get a general picture of the paleotemperature field reached by the Paleozoic series. Almost all lithologies were tested for the RSCM analysis. Several samples were polished at 35 µm for optical microscope observation (Fig. 6) but most of the measurements were carried out on 200–300µm-thick thin sections. The thin sections were prepared regardless of the mineral preferred orientation of the carbonaceous matter because of the poorly developed graphitization in these low metamorphic grade series (Aoya *et al.*, 2010).The RSCM method reliability depends on the richness of the carbonaceous matter enclosed in the sample. In the field, the dark lithologies, *i.e.* the Early Ordovician and Visean-Serpukhovian turbidites, turned out to be the most appropriate lithologies (Figs. 6a, 6b, 6d and 6f). On the contrary, the Early Cambrian Marcory green sandstone, and the Early Cambrian and Devonian carbonates did not yield sufficient organic matter (Figs. 6c and 6e), and thus, were avoided for sampling.

4.5 Sampling strategy

The main goal of the present study was to establish the paleotemperature field associated with the regional tectonic-metamorphic events. Several hypotheses may be formulated.

The temperature development was coeval with the recumbent folding and thrusting event for this purpose, samples were collected in each structural unit except for the South Minervois and Mts-de-Faugères units. Higher temperatures can be expected at deeper tectonic levels. Furthermore, areas distant from the Axial Zone dome where the metamorphic and structural imprint of the Axial Zone dome upon the recumbent folds seems absent (Doublier *et al.*, 2006) represent attractive sites. For instance, in the Ordovician sandstone-siltstone formation of the Upper (Pardailhan) recumbent fold, only the S1 slaty cleavage is observed (Fig. 4a).

The thermal effect was related to the late-stage emplacement of the migmatites and plutons in the Axial Zone dome. The strategy to assess the dome effect, as suggested by Wiederer *et al.* (2002) and Franke *et al.* (2011) studies, was totally different. In the southern flank, upright folds coeval with a steep S2 cleavage (Fig. 4b) structurally represents this event. The occurrence of a N70E striking mineral lineation marked by white mica (sericite) becomes more and more difficult to recognize south of the dome. Consequently, high temperatures should be recorded near the dome while they must decrease away from it, southwards. Nord-south sections were sampled in order to test this hypothesis.

Finally, a last possibility can be considered. The axial dome exhumation itself results of a regional horizontal flow that affected the entire crust. Thus, a hot crust could be located below the nappes piles. Beside the dome thermal impact, a high temperature event overprinting the nappe stacking can be expected far from the Axial Zone.

5 Results

Despite the low-grade metamorphism of the area, both high and low temperature methods were used during this study. The results are well distributed in the 230 to 400 °C range covered by both methods (Figs. 5 and 7). Seventy-two temperature values were calculated in the Montagne Noire southern flank. Forty-eight RSCM spectra were processed using Lahfid *et al.* (2010) method, while twenty-five spectra were computed through the Beyssac *et al.* (2002) method (Tab. 1). Thirty-six temperatures values were also reassessed by the FWHM-D1-linked thermometer (Kouketsu *et al.*, 2014; Tab. 2). The results, plotted in Figure 8, reveal a decreasing of maximum temperatures towards the south. It appears that the metamorphic zonation cuts across the boundaries between the tectonic units and the limbs of recumbent folds close to the dome and a more homogenous in further distance. In contrast to one of our working hypotheses, the RSCM temperatures do not indicate any thermal gap on both sides of the tectonic contacts.

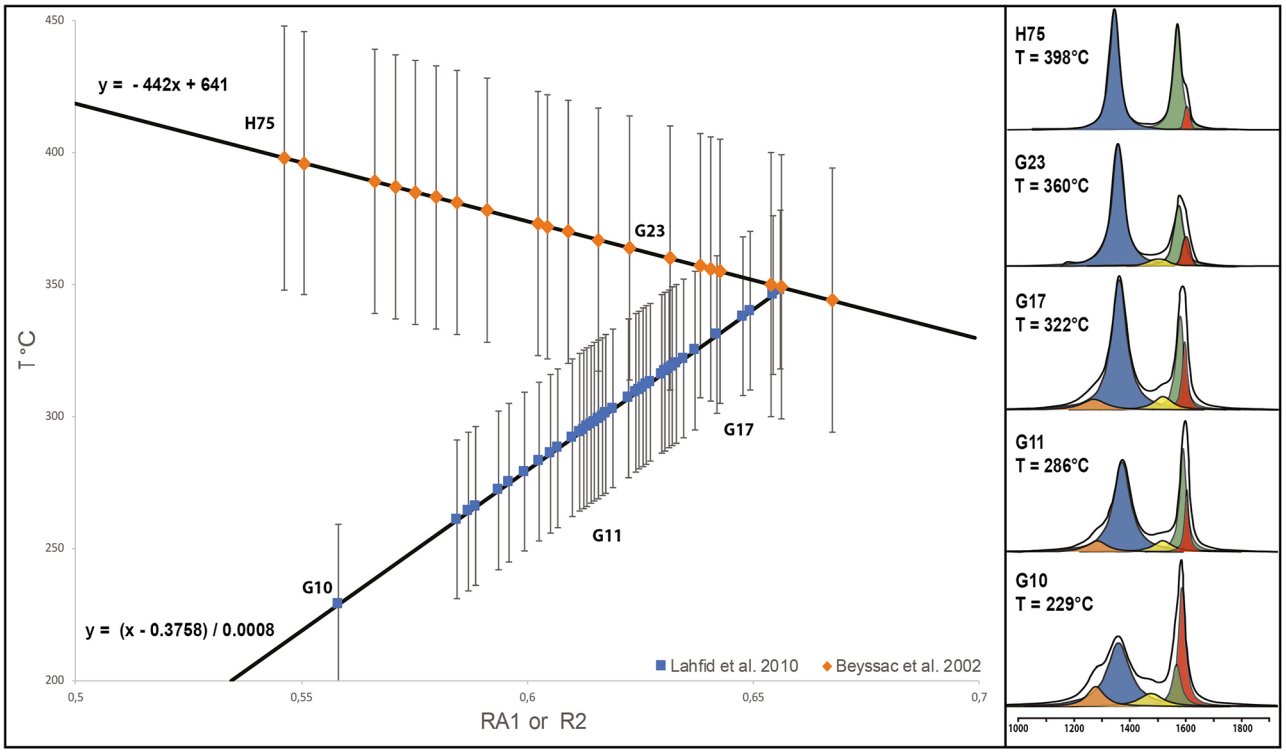

Fig. 7. Graph showing the repartition of our data with respect to the two methods used. The right column shows the evolution of the spectra aspect and the deconvolution chosen with D1 band (blue), D2 band (red), D3 band (yellow), D4 band (orange) and G band (green).

6 Discussion

6.1 Temperature field acquired by RSCM method

In this study, the entire Montagne Noire southern flank has been investigated by the RSCM method. Most of the data set obtained from the sedimentary rocks records a gradient consistent over the whole investigated area, visible in both normal and inverted sedimentary series (Fig. 8 and 9 cross sections 1, 2, 3, 4, 5). Globally, the temperature decreases from the southern edge of the Axial Zone dome towards the southeast in the Paleozoic sedimentary rocks (Fig. 10). The maximum temperature is located in the micaschists series that form the dome envelope with a value close to 400 °C. The lowest temperature, about 220 °C, was obtained in the Visean turbidites. In the western part of the southern flank, the gradient is less apparent that in the eastern part. It decreases from 400 °C to 315 °C towards the Cenozoic sedimentary rocks.

The RSCM method was also used within the dome micaschist envelope (Fréville *et al.*, 2016). The measured temperatures, ranging between 450 °C and 600 °C are higher than those obtained in the sedimentary rocks of the southern flank (Fig. 11). The temperature gradient is steeper in the dome northern edge than in the micaschist series of the eastern area. Indeed, the deformation is more intense in the dome northern edge, as also shown by the tight arrangement of the metamorphic isograds (Alabouvette *et al.*, 1993; Fréville *et al.*, 2016). This is probably a consequence of a brittle shearing that poste-dates the dome exhumation (Thompson and Bard, 1982). The data set obtained *via* the RSCM method documents a continuous evolution from the dome core southward with a temperature decrease from 580 °C to less than 300 °C (Fig. 11). Since the dome foliation is plunging under the sedimentary series, samples horizontally away from the dome are also vertically distant from the dome.

In case of a thermal field predating the emplacement of the recumbent folds, a temperature discontinuity should coincide with the contacts between different units. In case of a thermal event coeval with nappe thrusting and tectonic thickening, the gradient should be consistent with the structural position in the tectonic pile. Indeed, it has been shown that temperatures recorded in terrigenous sedimentary series deposited in foreland basins involved in fold-and-thrust belts of orogens are related to tectonic thickening. For instance, in the northern Variscan foreland basin of the Ardennes massif, the temperature of 200 to 300 °C, measured by illite crystallinity, vitrinite reflectance, conodont alteration index, and fluid inclusion methods, has been linked to the burial of sedimentary series below the Variscan thrust front (Fielitz and Mansy, 1999).

The RSCM temperature map of the Montagne Noire southern flank (Fig. 10) is clearly incompatible with these assumptions. Since the isotherms cut across the different fold units irrespective of their contacts, the bulk thermal structure of the Montagne Noire southern flank cannot be linked to the pre-doming thickening stage. Moreover, the RSCM temperature is not correlated with the structural position of the analyzed samples since the highest nappes of the tectonic pile record temperatures similar to those measured in the para-autochthonous units (Fig. 10). Thus, the link of the temperature field with nappe emplacement, and tectonic burial is unlikely. The measured temperature is also not in agreement with shear heating along major contacts, as that observed in Japan (Mori *et al.*, 2015).

Table 1. Tmax results obtained by RSCM according to Beyssac *et al.* (2002) and Lahfid *et al.* (2010) methods.

Sample	Longitude E	Latitude N	Age	Unit	Method	RA1 or R2	T°C	SD	r^2	N	N'
G1	2.8705744	43.5442683	Ordovician	LRF	HT	0.648	352	11	0.991	15	15
G2	2.8965896	43.5575776	Ordovician	LRF	HT	0.603	373	7	0.988	13	10
G3	2.8940602	43.5535283	Ordovician	LRF	HT	0.592	378	8	0.998	15	15
G4	2.9825362	43.5586861	Ordovician	LRF	HT	0.605	371	14	0.996	16	16
G5	2.9736861	43.5390556	Ordovician	LRF	HT	0.655	350	8	0.992	15	15
G6	3.0860833	43.5084722	Visean	LRF	LT	0.610	293	24	0.993	15	15
G7	3.1330833	43.5384167	Visean	FU	HT	0.626	362	14	0.994	15	15
G8	3.1730278	43.5589167	Visean	FU	HT	0.618	366	12	0.984	12	12
G9	3.1807778	43.5396389	Visean	VB	HT	0.631	364	16	0.99	12	12
G10	3.1667501	43.5195833	Visean	VB	LT	0.558	229	17	0.994	11	11
G11	3.1333333	43.52075	Visean	FU	LT	0.605	287	14	0.992	15	15
G12	3.1158333	43.4986944	Visean	FU	LT	0.597	276	12	0.994	15	15
G13	3.0292778	43.50825	Devonian	LRF	LT	0.616	300	16	0.992	13	12
G14	3.0304444	43.5108889	Visean	LRF	LT	0.620	305	16	0.995	10	10
G15	3.0316111	43.5126111	Visean	LRF	LT	0.617	302	24	0.991	12	12
G16	3.0378333	43.5198889	Visean	FU	LT	0.621	307	22	0.994	12	12
G17	3.0374166	43.5306389	Visean	FU	LT	0.634	323	20	0.996	11	10
G20	2.9909722	43.5338888	Visean	LRF	LT	0.649	341	29	0.995	16	16
G21	3.0191944	43.5502222	Visean	PA	HT	0.567	388	22	0.983	15	14
G22	2.8663334	43.51475	Ordovician	URF	LT	0.607	299	27	0.991	15	14
G23	2.8574722	43.5298055	Ordovician	URF	HT	0.612	369	23	0.993	15	15
H1	3.1719473	43.5422333	Visean	FU	LT	0.619	304	15	0.994	15	15
H2	3.1574222	43.5463472	Visean	FU	LT	0.631	319	16	0.996	15	15
H3	3.1426028	43.5478777	Visean	FU	HT	0.629	361	8	0.989	15	15
H4	3.111275	43.540825	Visean	FU	HT	0.640	356	5	0.993	15	15
H5	3.1088889	43.5347195	Visean	FU	HT	0.665	345	9	0.992	15	15
H6	3.1116833	43.5300195	Visean	FU	HT	0.657	349	9	0.989	15	15
H7	3.1185889	43.5235944	Visean	FU	HT	0.634	359	13	0.994	15	15
H9	3.0303112	43.5103778	Visean	LRF	LT	0.623	309	19	0.993	15	15
H10	3.0314056	43.5011778	Ordovician	LRF	LT	0.622	308	13	0.995	15	15
H11	2.9952277	43.5168361	Visean	LRF	LT	0.649	341	24	0.992	15	14
H12	2.9672362	43.5270528	Ordovician	LRF	LT	0.645	337	13	0.995	15	15
H13	2.9632639	43.5292139	Ordovician	LRF	LT	0.648	341	25	0.988	15	15
H14	2.9575749	43.511325	Ordovician	LRF	LT	0.620	305	27	0.991	15	15
H15	2.9796389	43.4680027	Ordovician	LRF	LT	0.587	264	16	0.992	15	15
H16	2.9540445	43.4954806	Ordovician	URF	LT	0.616	300	24	0.992	15	13
H17	2.9323777	43.4954694	Ordovician	URF	LT	0.618	303	26	0.988	15	14
H18	2.9235973	43.49065	Ordovician	URF	LT	0.628	315	27	0.992	15	15
H19	2.9149528	43.4943194	Ordovician	URF	LT	0.586	262	13	0.993	15	15
H21	2.9037889	43.4920527	Mid-Cambrian	URF	LT	0.627	314	24	0.992	15	15
H27	2.8315083	43.3985361	Ordovician	URF	LT	0.629	317	25	0.992	15	14
H28	2.8038	43.3956139	Ordovician	URF	LT	0.636	325	25	0.992	15	14
H29	2.7726888	43.3927805	Ordovician	URF	LT	0.641	331	14	0.992	15	15
H33	3.04814	43.48132	Ordovician	LRF	LT	0.589	267	23	0.994	15	15
H34	2.97411	43.47787	Ordovician	LRF	LT	0.603	284	21	0.992	15	15
H35	2.98153	43.45686	Ordovician	LRF	LT	0.599	280	9	0.993	15	15
H36	2.96578	43.44078	Ordovician	URF	LT	0.607	289	20	0.993	15	15
H37	2.96172	43.44911	Ordovician	URF	LT	0.646	300	9	0.994	15	15
H38	2.94512	43.44965	Ordovician	URF	LT	0.611	294	11	0.992	15	15
H39	2.95357	43.4395899	Ordovician	URF	LT	0.589	266	15	0.992	10	10
H40	2.9217201	43.4348399	Ordovician	URF	LT	0.592	270	19	0.993	15	15
H41	2.75068	43.4804	Devonian	PA	HT	0.562	391	15	0.995	15	15

Table 1. (continued).

Sample	Longitude E	Latitude N	Age	Unit	Method	RA1 or R2	T°C	SD	r^2	N	N'
H42	2.75775	43.46934	Ordovician	PA	LT	0.631	319	14	0.993	15	15
H44	2.73973	43.43944	Ordovician	URF	LT	0.617	302	14	0.993	15	15
H49	2.68464	43.39284	Low-Cambrian	URF	LT	0.635	323	9	0.995	15	15
H51	2.63116	43.39683	Mid-Cambrian	URF	LT	0.631	319	15	0.992	15	15
H52	2.63325	43.37185	Ordovician	URF	LT	0.616	301	22	0.993	15	15
H53	2.6186917	43.3603834	Ordovician	URF	LT	0.626	312	10	0.992	15	15
H54	2.52333	43.33182	Devonian	LRF	LT	0.632	320	13	0.995	15	15
H57	2.5240901	43.34533	Mid-Cambrian	LRF	LT	0.626	312	10	0.992	15	15
H62	2.4564	43.32259	Ordovician	LRF	LT	0.629	317	17	0.994	15	15
H65	2.45733	43.364	–	M	HT	0.571	387	13	0.996	15	15
H67	2.45521	43.32847	Mid-Cambrian	LRF	LT	0.642	332	18	0.994	15	15
H69	2.39389	43.31236	Ordovician	LRF	LT	0.623	308	9	0.994	15	15
H75	2.38119	43.35939	–	M	HT	0.544	399	10	0.992	15	15
H76	2.35966	43.34023	Low-Cambrian	LRF	HT	0.642	355	6	0.992	15	15
H81	2.34584	43.34154	–	M	HT	0.601	372	13	0.989	15	15
H85	2.3226	43.33332	–	M	HT	0.583	381	10	0.997	15	15
H91	2.3542701	43.3423599	Devonian	LRF	HT	0.569	388	21	0.985	15	15
H92	2.35912	43.35098	–	M	HT	0.601	374	27	0.976	15	13
H94	2.35903	43.34991	Devonian	PA	HT	0.549	397	18	0.995	15	15
M016A	3.14975	43.5287778	Visean	VB	LT	0.606	301	18	0.977	11	10

LT: low temperature method (Lahfid *et al.*, 2010), HT: High temperature method (Beyssac *et al.*, 2002). FU: Faugères Units; LRF: Lower Recumbent Fold; URF: Upper Recumbent Fold; PA: Para-Autochthonous; M: Micaschists; VB: Visean Basin. With SD: standard deviation; r^2: fitting parameters; N: number of total spectra; N' number of retained spectra.

In contrast, there is a clear temperature gradient decreasing with the distance to the dome. Whatever the thrusting direction of the nappe, southeastward (Arthaud, 1970) or northeastward (Chardon *et al.*, 2020), the interpretation of a thermal effect related to the Axial Zone dome is therefore preferred to explain the temperature field as suggested by previous authors (Wiederer *et al.*, 2002; Doublier *et al.*, 2006; Franke *et al.*, 2011). At first order, the RSCM method records the HT metamorphic event already recognized close to the Axial Zone over a very broad area including its entire southern flank. It has been shown that RSCM investigations around an intrusion provide high temperatures away from the metamorphic aureole (*e.g.* Hilchie and Jamieson, 2014; Beyssac *et al.*, 2019).

However, it is quite unlikely that the heat propagation away from the dome may develop temperatures above 300 °C as those observed south of St-Pons at ca 10 km in the southernmost part of the upper recumbent fold. We suggest that the temperature field is linked with an hypothetic hot crust below the recumbent folds.

6.2 Anomalies in the temperature field

Two temperature anomalies are visible within the N-S temperature gradient (Fig. 8). To the east of the study area, within the Visean-Serpukhovian turbiditic basin, several samples present relatively high temperatures around 360 °C, similar to those found near the dome micaschists (Figs. 6 and 9 cross section 5). However, in this area, the Axial Zone dome is not exposed. The other temperature anomaly is located in the southern part of the Pardailhan upper recumbent fold (Fig. 9 cross section 3). The gradient is decreasing southward from ca 380 °C to 270 °C, but at the very end of the exposed Paleozoic series, the temperature increases to reach ca 320 °C. Since this area is located about 15 km away from the Axial Zone dome south margin, it is unlikely that these high temperatures result from the direct dome thermal influence.

Three hypotheses might explain these singularities.

First, the effect of a late fault might be taken in account as it could reorganize the distribution of paleotemperatures. It is especially noticeable for the anomaly within the upper recumbent fold (Pardailhan unit). The N-S striking sinistral fault at the east of the points H25 an H26 Fig. 2) separates high temperature in the west > 315 °C (H27-H28-H29) from lower temperatures in the east < 290 °C (H36-H39-H40; Figs. 8 and 9). This effect is also shown by the bending of the 300 °C isotherm (Fig. 10).

Second, the circulation of fluids, related to the nappes thickening or the doming may be considered. Several quartz veins, developed during these circulations, appear within the basin and close to the tectonic contacts (Guiraud *et al.*, 1981) or are linked with the micaschist/sedimentary rocks contact as observed in Salsigne (Lescuyer *et al.*, 1973).

Finally, at the regional scale, the district is riddled by Late Carboniferous granitic intrusions, such as the Sidobre or Folat plutons (Fig. 2), thus the presence of a hidden pluton below the sedimentary rocks cannot be discarded. Granitic plutons

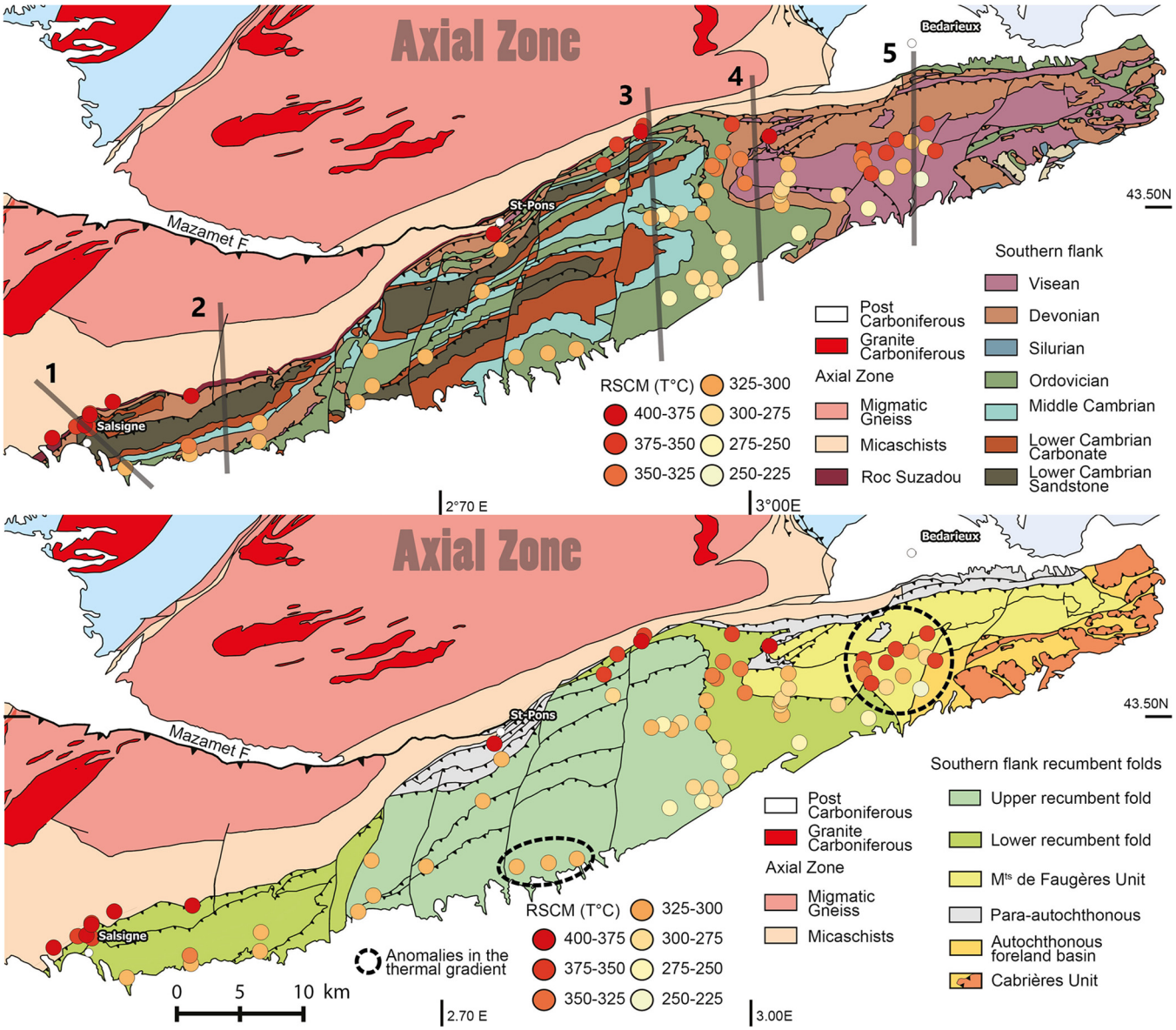

Fig. 8. Geological map of the Montagne Noire with the Tmax measured in the southern flank. Totally, 72 samples from the recumbent folds and turbiditic basin have been analysed by the RSCM method in the present study.

emplaced in an orogen external zone and in gneissic domes have been already documented in the Nappe and External zones of Sardinia (Carmignani *et al.*, 1994; Carosi *et al.*, 1998) and more recently by RSCM investigation in Morocco (Delchini *et al.*, 2016). Thus, the existence of several hidden gneiss-granite-migmatite massifs underlying the southern flank stack of recumbent folds and the turbiditic basin must be considered. Moreover, a pegmatite dyke, 2 km north of the anomaly in the basin, dated at 282 Ma (Doublier *et al.*, 2015), could be the witness of one of these intrusions. This hypothesis is closely related with the presence of a hot crust which can explain the isotherm pattern in the easternmost part of the southern flank, more than 15 km away from the dome (Fig. 10).

6.3 Comparison of the RSCM results with other thermometers

6.3.1 General pattern of the temperature field

The illite crystallinity has been widely studied in the eastern part of the Montagne Noire southern flank to unravel low-grade metamorphic gradients. In our study area, two previous works (Engel *et al.*, 1980-1981; Doublier *et al.*, 2015) documented a north to south decreasing thermal gradient (Fig. 12). The latter study used the Árkai index (Árkai, 1991; Guggenheim *et al.*, 2002) and the Kübler index (Kübler, 1964) to estimate a relative indicator of temperature. Furthermore, Wiederer *et al.* (2002) compared the results obtained *via* the Weber index (Weber 1972) in Engel *et al.* (1980-1981) to the

Table 2. Tmax results obtained by RSCM according to Kouketsu *et al.* (2014) method.

Sample	P D1	FWHM D1	T °C	SD	r^2	N'
H1	1344	94	275	19	0.998	15
H2	1352	55	360	8	0.998	15
H3	1352	51	367	5	0.995	15
H4	1354	49	373	7	0.994	15
H5	1351	53	365	11	0.995	15
H6	1351	52	367	9	0.996	15
H7	1352	55	360	15	0.998	15
H9	1345	85	296	12	0.997	15
H10	1342	96	272	7	0.999	15
H11	1350	68	332	18	0.994	15
H12	1350	75	318	10	0.998	15
H13	1347	74	319	8	0.998	15
H14	1345	99	265	22	0.998	14
H15	1344	104	255	14	0.995	15
H33	1345	107	248	14	0.998	15
H34	1342	99	265	13	0.997	15
H35	1346	107	248	8	0.998	15
G2	1354	47	377	8	0.987	13
G3	1354	42	389	3	0.998	15
G4	1355	45	380	2	0.997	16
G5	1352	61	347	7	0.996	15
G6	1344	83	300	20	0.998	15
G7	1351	53	364	7	0.997	15
G8	1353	46	379	8	0.996	12
G9	1353	52	367	12	0.997	12
G10	1348	106	249	8	0.998	11
G11	1345	89	286	19	0.998	15
G12	1348	95	291	11	0.994	10
G13	1347	77	312	17	0.996	15
G14	1348	71	325	16	0.999	10
G15	1349	70	327	12	0.998	12
G16	1350	67	333	13	0.998	12
G17	1352	59	352	14	0.998	11
G20	1352	59	351	13	0.997	16
G21	1353	50	371	12	0.994	15
MO16	1343	80	305	11	0.999	11

P_D1: stands for the band position (cm^{-1}); FWHM: Full Width at Half Maximum (cm^{-1}); SD: standard deviation; r^2: fitting parameters; N': number of retained spectra.

diagenetic domains defined in Frey and Robinson, (1999). In agreement with our own results, these works show the same N-S variations as those documented by the RSCM method.

In the same area, the conodont color alteration has been used to estimate the paleotemperature repartition (Wiederer *et al.*, 2002). The method is based on the color of apatite crystals that form the conodonts (Epstein *et al.*, 1977). During a metamorphic event, the crystallinity of organic matter trapped within the apatite grains increases, allowing a possible correlation with the metamorphic grade experienced by the fossil. As shown in Figure 13, the dome thermal effect is also visible by this method. The intensity of the metamorphism is globally higher to the northwest and decreases away to the southeast (Fig. 13).

A fluid inclusion study of quartz veins (see location on Fig. 11) has been carried out (Guiraud *et al.*, 1981). The analyzed rocks lie along the basal tectonic contact of the Pardailhan upper recumbent fold, called "queue de cochon" (pig tail) contact (Gèze, 1949) composed of Devonian limestone boudins surrounded by Ordovician sandstone and pelite. These 1- to 10-cm sized quartz lenses were inferred to be related to fluid circulation coeval with the emplacement of the upper recumbent fold (Guiraud *et al.*, 1981). Analyses show a temperature around 275 ± 25 °C, which is in agreement with our results at ca 300 °C, but higher than those provided by illite crystallinity at 200 °C (Doublier *et al.*, 2015). This 300 °C temperature has been related to the thickening event (Guiraud *et al.*, 1981), however, fluid circulation might have occurred

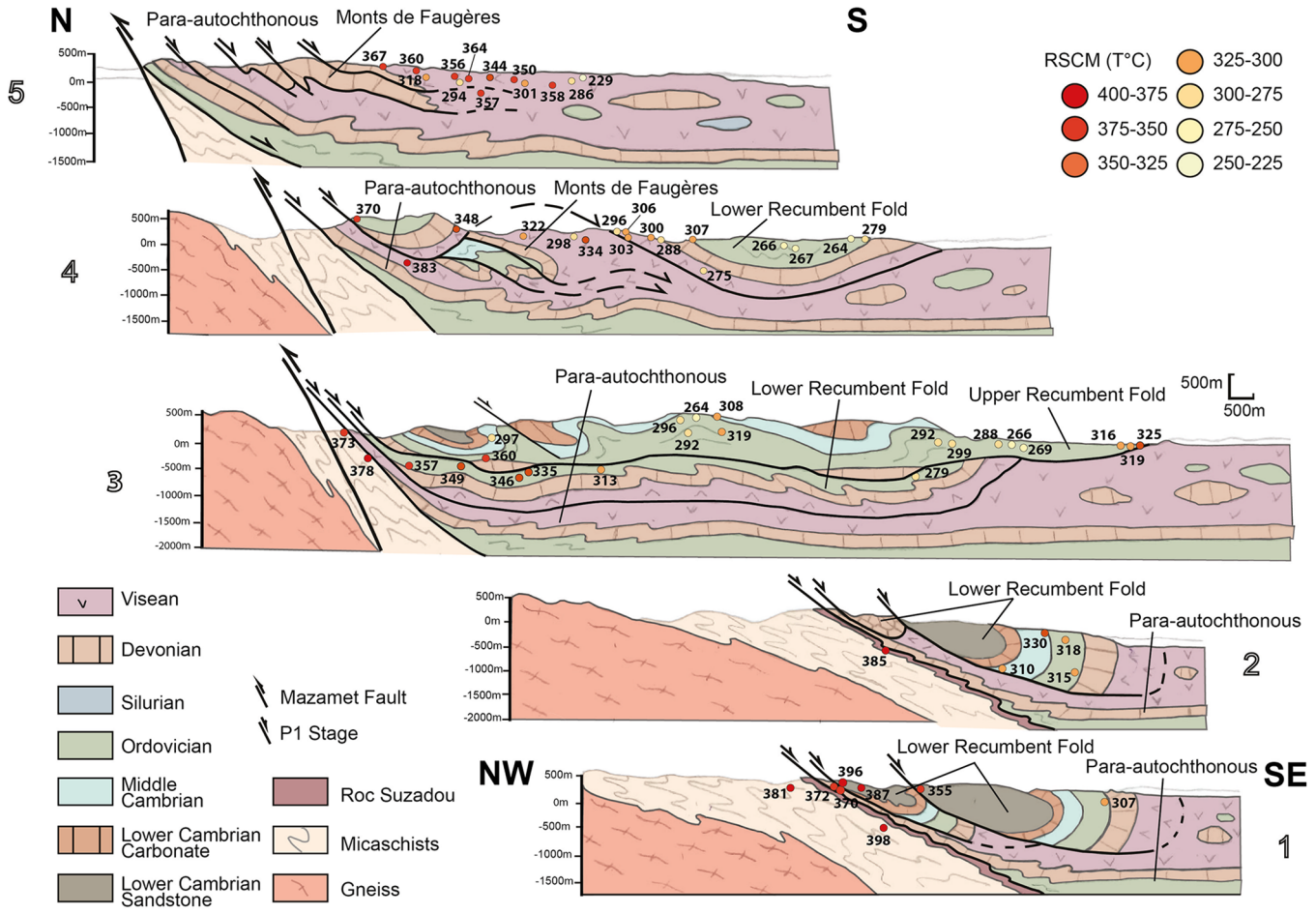

Fig. 9. Projections of the analyzed samples on five cross sections (located in Fig. 8) of the southern flank of the Montagne Noire. Temperatures are globally increasing toward the Axial Zone dome.

also during the doming. The tectonic contact between the upper and lower recumbent folds has been reworked during doming, as indicated by E-W striking slickenlines on flat lying surfaces, and N70E striking fibers infilling tension gashes (Arthaud, 1970; Sauniac, 1980; Harris *et al.*, 1983). Therefore, the deformation observed along the contact suggests that the ca 300 °C temperature might be related to the Axial Zone dome thermal effect or even to a late event as documented by Aerden (1998) and Franke *et al.* (2011).

6.3.2 Discrepancy in the low T range between RSCM temperature and other thermometers

For the sake of comparison between the different geothermometers, both conodont color alteration index and illite crystallinity data were converted in temperatures using to the tables provided by Merriman and Frey (1999) and Wiederer *et al.* (2002) for low grade metamorphism and the equation (1) from Zhu *et al.* (2016) work. Several studies have shown a good correlation between illite crystallinity (IC, estimated from Kübler Index, KI) and organic geothermometers such as vitrinite reflectance (VR) (Underwood *et al.*, 1993; Mukoyoshi *et al.*, 2009; Fukuchi *et al.*, 2014). This is true in basinal settings (Baludikay *et al.*, 2018) but also in collision/subduction settings (Rahn *et al.*, 1995). In the Montagne Noire, and despite qualitatively convergent trends indicating a north-south gradient from the Axial Zone dome to the sedimentary southern flank, the measured temperatures vary significantly, depending on the method considered.

As example of these differences, the temperature range estimated using the conodont approach is the widest, with temperatures comprised between 75 °C and 475 °C against 85 °C to 300 °C for IC and 230 °C to 400 °C for RSCM. Furthermore, for a given location, the results are sometimes different between the two illite crystallinity studies by Engel *et al.* (1980-1981) and Doublier *et al.* (2015). This is remarkable at the contact between the lower recumbent fold and the Visean basin where the data from Engel *et al.* (1980-1981) are 50 °C higher than those from Doublier *et al.* (2015). It can be explained by the use of a standardized and more precise procedure in the study of Doublier *et al.* (2015) while Engel *et al.* (1980-1981) employed an early version of the method known to have interlaboratory standardization issues (Merriman and Peacor, 1999). Comparing with RSCM result, other geothermometers provide temperature lower by at least 70 °C. Baludikay *et al.* (2018) reported a general overestimation of RSCM temperatures (using Kouketsu *et al.*, 2014 calibration) with respect to other geothermometer in low-grade sediments ($T < 200$ °C) from intra-cratonic basins. The discrepancy is here much higher, as illite crystallinity data

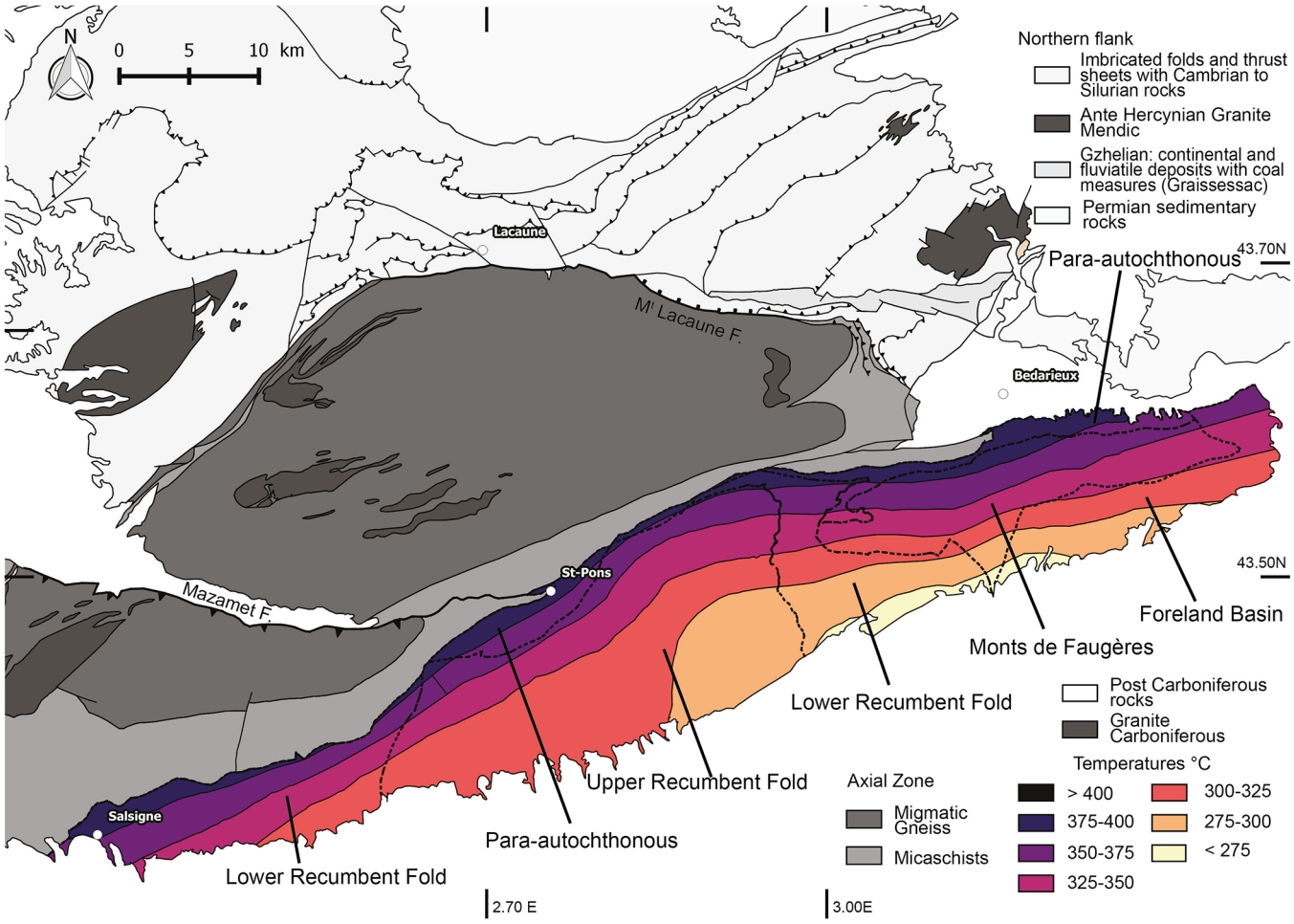

Fig. 10. Temperature map determined by the RSCM Tmax results of this study. The isotherms crosscut the tectonic units of the southern flank. Roughly, the temperature decreases from the NW to the SE away from the Axial Zone dome. The isotherms cut the micaschists between Salsigne and St-Pons because of a lack of data.

from Doublier *et al.* (2015) and RSCM data from this study show a difference up to 175 °C (Fig. 14). A first possible source of these differences lies in the large uncertainty in the conversion of any of the metamorphic/organic indicators into temperatures. A second source of error is related to the complex geological history of the domain treated here, involving several tectonic and heating stages, which might have affected to a variable extent the organic and mineral signals (García-López *et al.*, 2001).

Nonetheless, irrespective of the comparison between temperatures themselves, there are also large differences in the temperature gradients derived from the different geothermometers. Between 1 to 6 km away from the dome, the illite crystallinity seems to reach a plateau around 275 °C (dashed line in Fig. 14). This plateau could correspond to the temperature above which small muscovite or sericite have completely replaced the original clays and would be the upper limit of the method, while carbonaceous matter crystallinity (hence its Raman spectra) continue its evolution at higher temperature. Hence, for comparing the RSCM temperature with illite crystallinity temperature, we shall exclude the highest temperature domain in the vicinity of the dome and consider the section at a distance from 5 km to 15 km from the dome. In this distance range, the gap between RSCM temperatures and illite crystallinity temperatures increases with the distance to the dome (Fig. 14). This divergence is apparently irrespective of the RSCM calibration used (Figs. 15a and 15b) or the calibration to convert KI in temperature (T):

- (i) With Merriman and Frey (1999) table: the difference between KI-derived and RSCM-derived temperatures varies from ~75 °C to ~150 °C (Lahfid *et al.*, 2010) and from ~80 °C to ~120 °C (Kouketsu *et al.*, 2014) at 5 km and 14 km from the dome, respectively.
- (ii) With Zhu *et al.* (2016) equation: the T difference varies from ~75 °C to ~175 °C (Lahfid *et al.*, 2010) and from ~80 °C to ~150 °C (Kouketsu *et al.*, 2014) in the same section.

Therefore, these disparities suggest that organic matter record the dome exhumation thermal impact on a much broader area than illite crystallinity.

To interpret these discrepancies, one has to consider the nature of the physical and chemical processes involved in

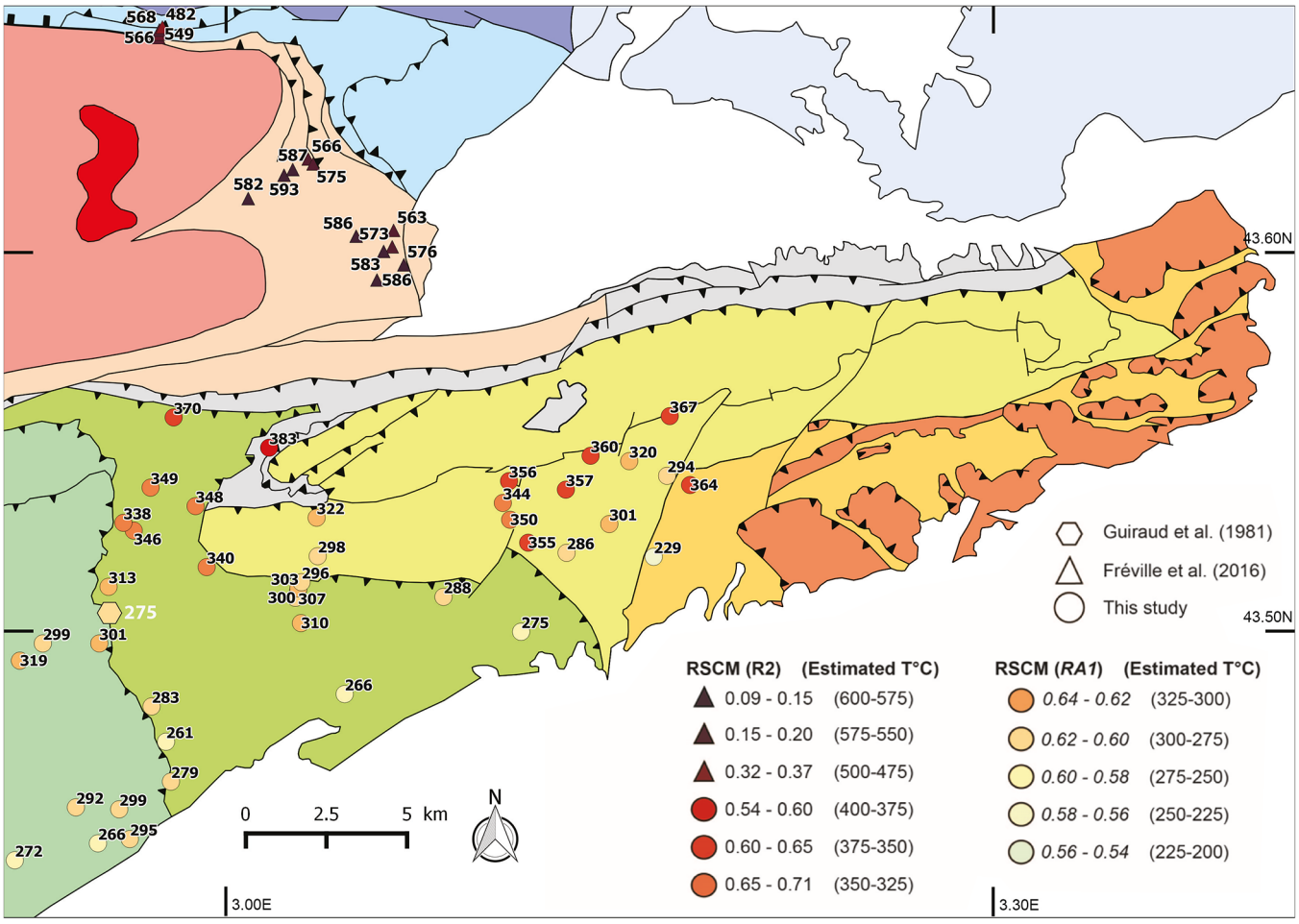

Fig. 11. Comparison of temperatures in °C acquired *via* RSCM method in this study and Fréville *et al.* (2016) and Guiraud *et al.* (1981) temperature from fluid inclusion.

carbonaceous matter and illite maturation. Velde and Lanson (1993), Belmar *et al.* (2002) and Mählmann *et al.* (2012) suggested that the carbonaceous matter records short thermal episodes, such as magmatic intrusions, more easily than clays. This contrasted record could be linked to the fact that organic matter maturation beyond its low-T cracking is principally isochemical, while illite and other clays evolution requires chemical reactions involving elemental exchanges (Velde and Lanson, 1993). The samples used to calibrate RSCM with illite crystallinity (Kouketsu *et al.*, 2014) were collected in an accretionary complex in SW Japan (Hara *et al.*, 2013). In this regional metamorphism context, both illite and carbonaceous material had sufficient time to maturate and tend towards some "equilibrium" state. With a duration longer than 10 Ma, several geothermometers based on various mineralogical assemblages yield the same temperature (Le Bayon *et al.*, 2011; Mullis *et al.*, 2017).

Hence, the disparities between illite crystallinity and RSCM in Montagne Noire suggest that the dome emplacement, which controls IC and RSCM evolution, was a relatively short event in terms of heat source. Accordingly, it left a more significant imprint on carbonaceous matter than on illite.

One can note that the much smaller-scale T anomaly in the basin, recorded by RSCM but not by illite crystallinity, can be similarly explained by hidden magmatic bodies that provided a local heat source for a short period of time. We therefore propose that a regional high heat-flow linked to a hot crust is present over a long period 330–295 Ma, as recorded by IC and CAI. However, local events resulting from this regional heat such as plutonic intrusion and on a larger scale the migmatization mostly affected the carbonaceous material.

Moreover, the high RSCM, IC and CAI temperatures observed in the basin far from the eastern terminaison of the dome suggest that a sinistral movement occurred during the dome emplacement. It is then possible that the tectonic origin of the dome emplacement took place during a sinistral transpression as suggested by Chardon *et al.* (2020). This view is also in agreement with a N-S shortening responsible for the double anticline present within the Axial Zone dome (Matte *et al.*, 1998; Malavieille, 2010).

7 Conclusion

The 72 RSCM measurements acquired in this study combined with the results of several previous studies, derived from different methods, allow us to reconstruct the thermal history of the Montagne Noire southern flank. The RSCM measurements, processed either by Lahfid *et al.* (2010) or

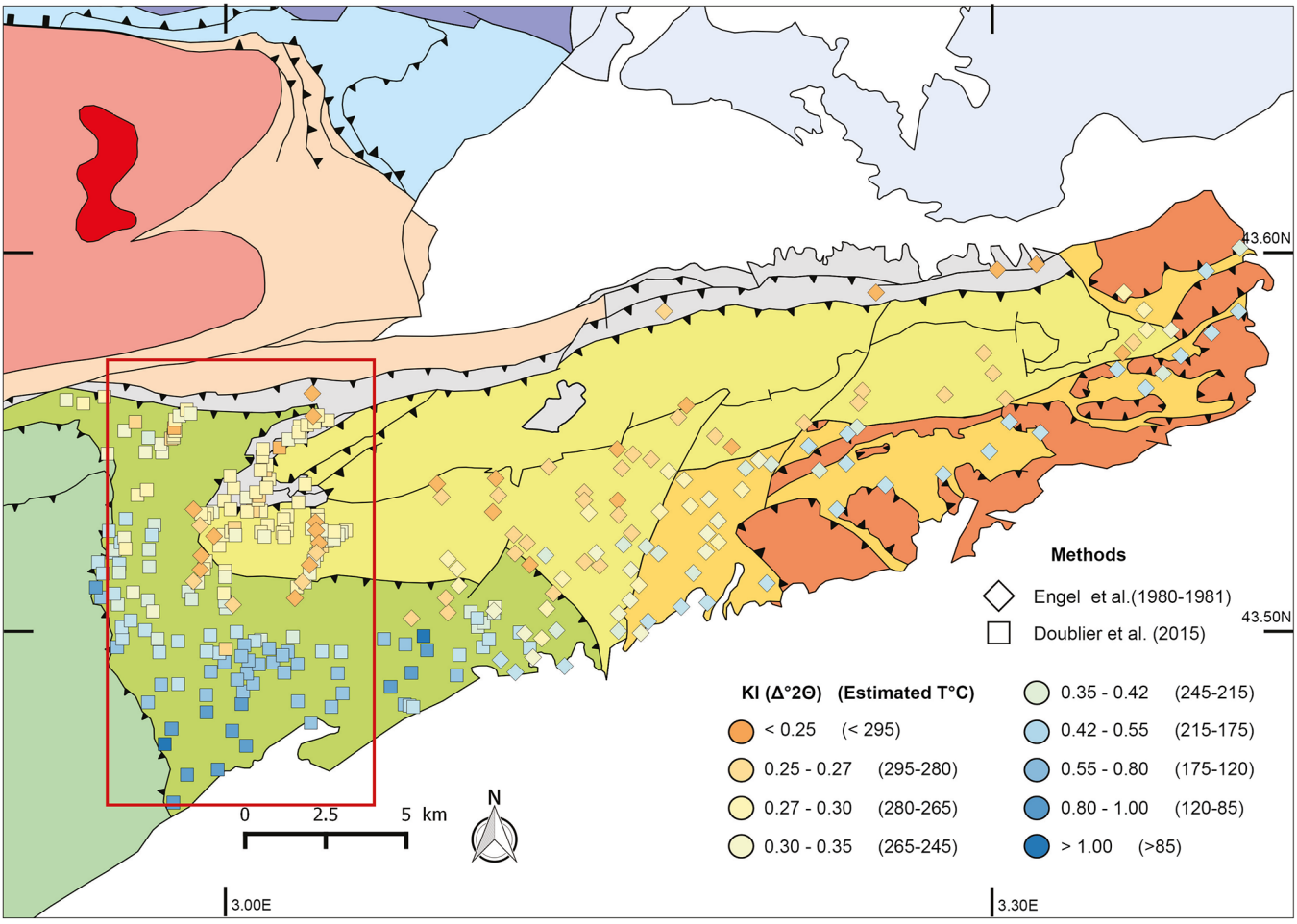

Fig. 12. Illite crystallinity data from previous studies (Engel *et al.*, 1981; Doublier *et al.*, 2015) based on the crystalline organization of illite analysed *via* X-ray diffraction converted from the Kübler index into °C (Merriman and Frey, 1999; Zhu *et al.*, 2016). The Figure 14 is based on the data from the red rectangle.

Beyssac *et al.* (2002) methods, cover the whole metamorphic range present in the sedimentary rocks. In agreement with the RSCM results, the conodont color alteration, and the illite crystallinity geothermometers revealed a temperature gradient within the Paleozoic formations decreasing from the Axial Zone dome toward the SE. This RSCM temperature gradient represents the effect of the Axial Zone dome overprint on the sedimentary rocks as suggested by previous studies on a smaller area (Engel *et al.*, 1980-1981; Wiederer *et al.*, 2002; Doublier *et al.*, 2015) and also observed in the Montagne Noire northern side (Doublier *et al.*, 2006).

Moreover, an underneath heating by the hot crust might also explain the relatively high temperatures, $>300\,^{\circ}C$, recorded by RSCM, IC and CAI in the very southern part of the upper recumbent fold and in the east of the southern flank.

In spite of a common North to South decreasing temperature gradient, the different thermometers present quantitative discrepancies in the estimated temperature. IC temperatures decrease away from the dome to temperatures below 150 °C, while RSCM temperatures remain above 250 °C. In this case, the fast kinetics of carbonaceous material crystalline evolution, with respect to illite crystalline evolution, could then account for the record of the heating event over a larger area by RSCM than by IC.

The link between the bulk temperatures and the recumbent folding is not supported by this study. Furthermore, anomalies are observed within the thermal gradient. Since these anomalies are not documented by the IC method, the most likely explanation would be that hidden bodies such as granitic plutons, would have emplaced beneath the Paleozoic sediments after the dome exhumation. In addition, the presence of a hot crust underlying the Paleozoic series cannot be discarded.

Finally, the temperatures obtained in the southern part of the Upper recumbent fold, alike those measured by fluid inclusion study (Guiraud *et al.*, 1981), are compatible with the Axial Zone doming. The RSCM approach suggests that the thermal effects related to the thickening event have been totally overprinted by the dome thermal effect.

As already investigated in the Rheno-Hercynian zone in the northern Variscan branch (*e.g.* Fielitz and Mansy, 1999; Doublier *et al.*, 2012), the study of thermicity in foreland basins can be extended to other areas within the Variscan belt. For instance, Mouthoumet massif (Kretschmer *et al.*, 2015),

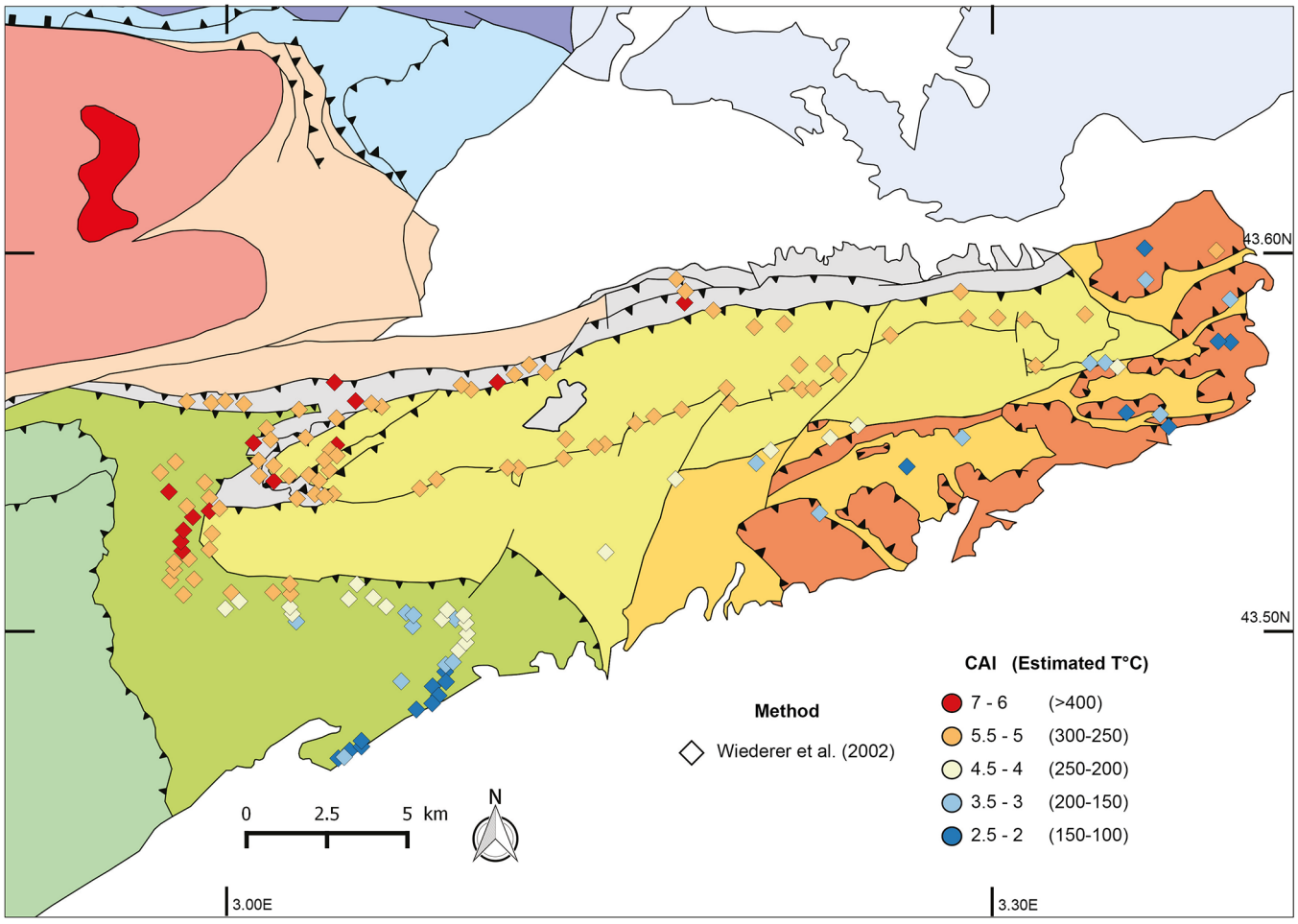

Fig. 13. Conodont alteration index method from previous study (Wiederer *et al.*, 2002). The colour of apatite crystals indicates its metamorphic degree. Wiederer *et al.* (2002) have studied more than three hundred conodonts.

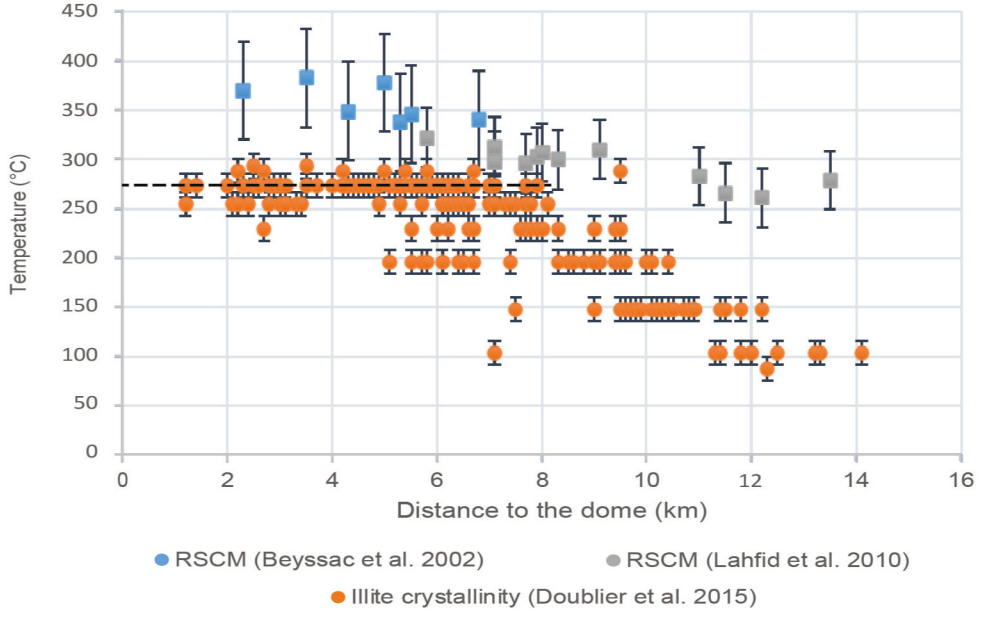

Fig. 14. Plot of the variation of measured temperatures using different methods with respect to the distance to the dome.

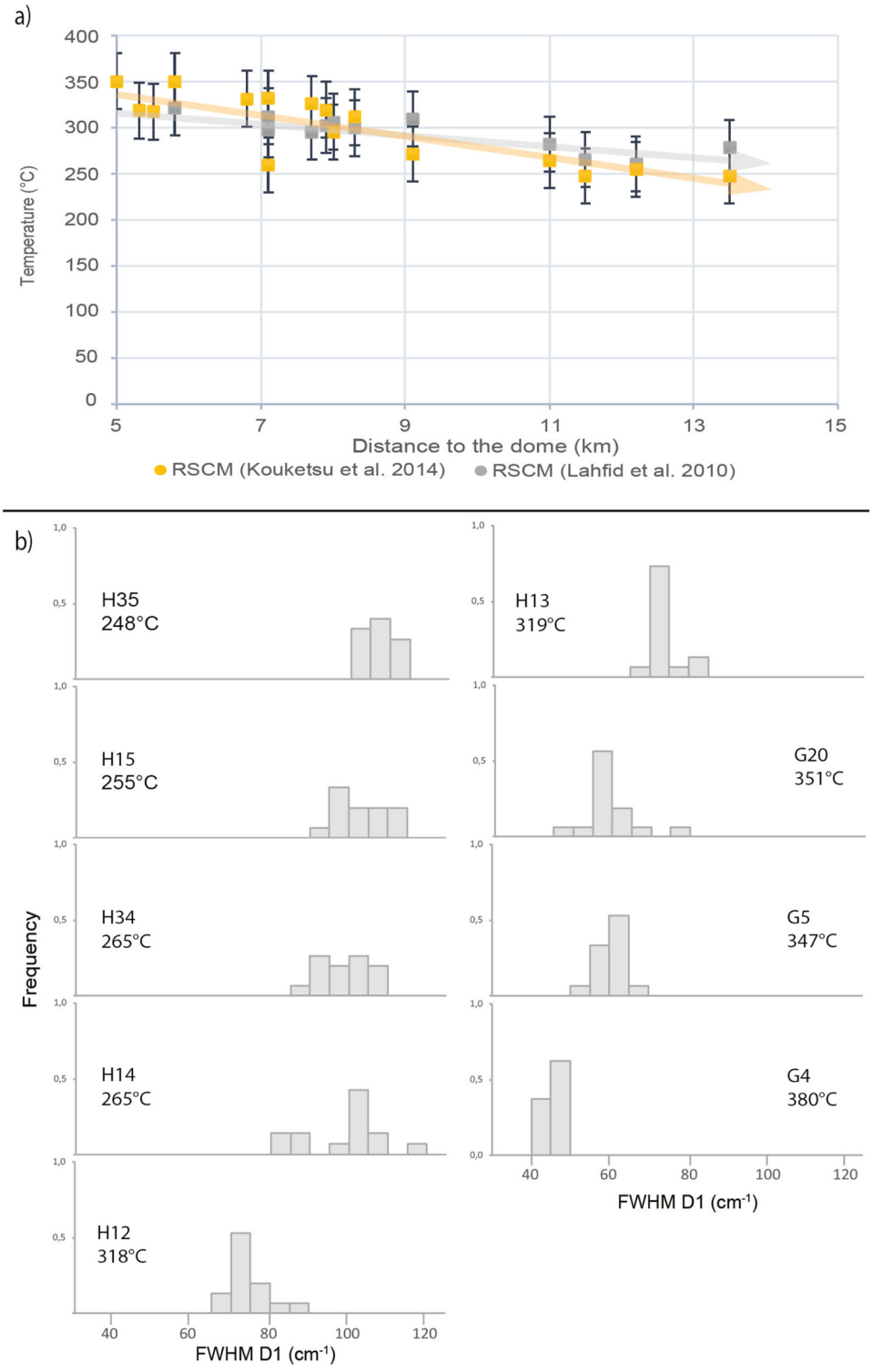

Fig. 15. (a) Comparison of Lahfid *et al.* (2010) and Kouketsu *et al.* (2014) thermometers, arrows represent the major linear trends. (b) Histograms of frequencies of the full width at half maximum of the band D1 (FWHM) acquired using the Kouketsu *et al.* (2014) method.

Balearic or southern Sardinia areas are suitable places to get a general picture of the Variscan thermicity.

Acknowledgments. This study has been funded by the Labex VOLTAIRE, and the Observatoire des Sciences de l'Univers en Région Centre (OSUC). Jean-Gabriel Badin, Sylvain Janiec, and Ida di Carlo are thanked for their assistance during the thin section preparation and Raman spectroscopy measurements. We aslo thank Stanislas Sizaret for his help during sampling session. Constructive comments by J. Malavieille, R. Carosi, and an anonymous reviewer are deeply acknowledged.

References

Aerden DG. 1998. Tectonic evolution of the Montagne Noire and a possible orogenic model for syncollisional exhumation of deep rocks, Variscan belt, France. *Tectonics* 17(1): 62–79.

Alabouvette B, Arthaud F, Bambier A, Freytet P, Paloc H. 1982. Notice explicative de la carte géologique au 1/50 000 de Saint-Chinian, n° 1014. Orléans, France : Bureau de Recherches Géologiques et Minières, pp. 1–44.

Alabouvette B, Demange M, Sauvel C, Vautrelle C. 1993. Notice explicative de la feuille Saint-Pons à 1/50 000. Orléans : Édition du Bureau de Recherches Géologiques et Minières.

Alabouvette B, Demange M, Guérangé-Lozes J, Ambert P. 2003. Notice explicative de la carte géologique au 1:250 000 de Montpellier. Orléans, France : Bureau de Recherches Géologiques et Minières.

Álvaro JJ, Vizcaïno D. 1998. Révision biostratigraphique du Cambrien moyen du versant méridional de la Montagne Noire (Languedoc, France). *Bulletin de la Société géologique de France* 169(2): 233–242.

Álvaro JJ, Courjault-Radé P, Chauvel JJ, Dabard MP, Debrenne F, Feist R, *et al.* 1998. Nouveau découpage stratigraphique des séries cambriennes des nappes de Pardailhan et du Minervois (versant sud de la Montagne Noire, France). *Géologie de la France* 2: 3–12.

Aoya M, Kouketsu Y, Endo S, Shimizu H, Mizukami T, Nakamura D, *et al.* 2010. Extending the applicability of the Raman carbonaceous-material geothermometer using data from contact metamorphic rocks. *Journal of Metamorphic Geology* 28: 895–914

Árkai P. 1991. Chlorite crystallinity: an empirical approach and correlation with illite crystallinity, coal rank and mineral facies as exemplified by Palaeozoic and Mesozoic rocks of northeast Hungary. *Journal of Metamorphic Geology* 9: 723–734.

Arthaud F. 1970. Etude tectonique et microtectonique comparée de deux domaines hercyniens : les nappes de la Montagne Noire (France) et l'anticlinorium de l'Iglesiente (Sardaigne). Université des Sciences et Techniques du Languedoc, 175 p.

Baludikay BK, François C, Sforna MC, Beghin J, Cornet Y, Storme JY, *et al.* 2018. Raman microspectroscopy, bitumen reflectance and illite crystallinity scale: comparison of different geothermometry methods on fossiliferous Proterozoic sedimentary basins (DR Congo, Mauritania and Australia). *International Journal of Coal Geology* 191: 80–94.

Bard JP, Rambeloson R. 1973. Métamorphisme plurifacial et sens de variation du degré géothermique durant la tectogenèse polyphasée hercynienne dans la partie orientale de la zone axiale de la Montagne Noire (Massif du Caroux, Sud du Massif Central français). *Bulletin de la Société géologique de France* 7(5-6): 579–586.

Berger G, Alabouvette B, Guérangé-Lozes J, Demange M, Ambert P. 2001. Carte géol. France (1/250 000), feuille Montpellier (38). Orléans : BRGM. Notice explicative par B. Alabouvette, M. Démange, J. Guérangé-Lozes, P. Ambert (2003), 164 p.

Beyssac O, Goffé B, Chopin C, Rouzaud JN. 2002. Raman spectra of carbonaceous material in metasediments: A new geothermometer. *Journal of Metamorphic Geology* 20: 859–871.

Beyssac O, Pattison DRM, Bourdelle F. 2019. Contrasting degrees of recrystallization of carbonaceous material in the Nelson aureole, British Columbia and Ballachulish aureole, Scotland, with implications for thermometry based on Raman spectroscopy of carbonaceous material. *J. Metamorphic Geol.* 37: 71–95.

Belmar M, Schmidt ST, Frey M, Ferreiro-Mählmann R, Mullis J, Stern W. 2002. Diagenesis, low-grade and contact metamorphism in the Triassic-Jurassic of the Vichuquén-Tilicura and Hualané-Gualleco Basins, Coastal Range of Chile. *Schweizeriche Mineralogische und Petrographische Mitteilungen* 82: 375–392.

Carmignani L, Carosi R, Di Pisa A, Gattiglio M, Musumeci G, Oggiano G, *et al.* 1994. The hercynian chain in Sardinia (Italy). *Geodinamica Acta* 7(1): 31–47.

Carosi R, Perillo M, Pertusati PC. 1998. Structural evolution of the Southern Sulcis Metamorphic Complex (SW Sardinia, Italy). *C. R. Acad. Sci. Paris, Sciences de la terre et des planètes/Earth & Planetary Sciences* 326: 505–512, Paris, Elsevier Gauthier-Villars.

Chardon D, Aretz M, Roques D. 2020. Reappraisal of Variscan tectonics in the southern French Massif Central. *Tectonophysics* 787.

Cocherie A, Baudin T, Autran A, Guerrot C, Fanning CM, Laumonier B. 2005. U-Pb zircon (ID-TIMS and SHRIMP) evidence for the early Ordovician intrusion of metagranites in the late Proterozoic Canaveilles Group of the Pyrenees, and the Montagne Noire (France). *Bull. Société géologique de France* 176: 269–282.

Cózar P, Izart A, Vachard D, Coronado I. 2017 A mid-Tournaisian-late Viséan carbonate ramp reconstructed from nappes and olistolites in the southern Montagne Noire (France). *Sedimentary Geology* 358: 148–175.

Delchini S, Lahfid A, Plunder A, Michard A. 2016. Applicability of the RSCM geothermometry approach in a complex tectono-metamorphic context: The Jebilet massif case study (Variscan Belt, Morocco). *Lithos* 256: 1–12.

Demange M. 1982. Etude géologique du massif de l'Agoût, Montagne Noire, France. Thèse d'Etat, Paris 6, 1050 p.

Demange M. 1993. Que signifie la faille des Monts de Lacaune (Montagne Noire, France) ? Implications quant au problème de la patrie des nappes. *Comptes rendus de l'Académie des sciences, Série 2*, 317: 411–418.

Doublier MP, Potel S, Wemmer K. 2006. Age and grade of metamorphism in the eastern Monts de Lacaune-implications for the collisional accretion in Variscan externides (French Massif Central). *Geodinamica Acta* 19: 391–407.

Doublier MP, Potel S, Franke W, Roache T. 2012. Very low-grade metamorphism of Rhenohercynian allochthons (Variscides, Germany): facts and tectonic consequences. *International J. Earth Sciences* 101: 1229–1252.

Doublier MP, Potel S, Wemmer K. 2015. The tectono-metamorphic evolution of the very low-grade hangingwall constrains two-stage gneiss dome formation in the Montagne Noire (Southern France). *Journal of Metamorphic Geology* 33: 71–89.

Dunoyer de Segonzac G, Ferrero J, Kübler B. 1968. Sur la cristallinité de l'illite dans la diagenèse et l'anchimétamorphisme. *Sedimentology* 10: 137–143.

Echtler H, Malavieille J. 1990. Extensional tectonics, basement uplift and Stephano-Permian collapse basin in a late Variscan metamorphic core complex (Montagne Noire, Southern Massif Central). *Tectonophysics* 177: 125–138.

Engel W, Feist R, Franke W. 1978. Synorogenic gravitational transport in the Carboniferous of the Montagne Noire (S-France). *Zeitschrift der deutschen geologischen Gesellschaft* 461–472.

Engel W, Feist R, Franke W. 1980-81. Le Carbonifère anté-stéphanien de la Montagne Noire: rapports entre mise en place des nappes et sédimentation. *Bull. BRGM.* 2: 341–389.

Epstein AG, Epstein JB, Harris LD. 1977. Conodont color alteration: an index to organic metamorphism. *Geological Survey of America, Professional Paper* 995: 1–27.

Faure M. 1995. Late orogenic carboniferous extensions in the Variscan French Massif Central. *Tectonics* 14: 132–153.

Faure M, Cottereau N. 1988. Données cinématiques sur la mise en place du dôme migmatique carbonifère moyen de la zone axiale, de

la Montagne Noire (Massif Central, France). *Comptes rendus Acad. Sci. Série 2* 307: 1787–1794.

Faure M, Bé Mézème E, Duguet M, Cartier C, Talbot JY. 2005. Paleozoic tectonic evolution of medio-Europa from the example of the French Massif Central and Massif Armoricain. *Journal of the Virtual Explorer* 19: 1–25.

Faure M, Lardeaux JM, Ledru P. 2009. A review of the pre-Permian geology of the Variscan French Massif Central. *Comptes Rendus Geoscience* 341: 202–213.

Faure M, Cocherie A, Bé Mézème E, Charles N, Rossi P. 2010. Middle Carboniferous crustal melting in the Variscan belt: New insights from U-Th-Pb tot monazite and U-PB zircon ages of the Montagne Noire Axial Zone (southern French Massif Central). *Gondwana Res.* 18: 653–673.

Faure M, Cocherie A, Gaché J, Esnault C, Guerrot C, Rossi P, *et al.* 2014. Middle Carboniferous intracontinental subduction in the Outer Zone of the Variscan belt (Montagne Noire Axial Zone, French Massif Central): multimethod geochronological approach of polyphase metamorphism. Multimethod geochronological approach of polyphase metamorphism. *Geological Society, London, Special Publications* 405(1): 289–311.

Faure M, Li XH, Lin W. 2017. The northwest-directed "Bretonian phase" in the French Variscan Belt (Massif Central and Massif Armoricain): a consequence of the Early Carboniferous Gondwana-Laurussia collision. *C. R. Géoscience* 349: 126–136.

Feist R, Galtier J. 1985. Découverte de flores d'âge namurien probable dans le flysch à olistolites de Cabrières (Hérault). Implication sur la durée de la sédimentation synorogénique dans la Montagne Noire (France méridionale). *Comptes Rendus Acad. Sciences, Série 2* 300: 207–212.

Fielitz W, Mansy JL. 1999. Pre-and synorogenic burial metamorphism in the Ardenne and neighbouring areas (Rhenohercynian zone, central European Variscides). *Tectonophysics* 309: 227–256.

Franke W, Doublier MP, Klama K, Potel S, Wemmer K. 2011. Hot metamorphic core complex in a cold foreland. *International Journal of Earth Sciences* 100: 753–785.

Fréville K, Cenki-Tok B, Trap P, Rabin M, Leyreloup A, Régnier JL, *et al.* 2016. Thermal interaction of middle and upper crust during gneiss dome formation: Example from the Montagne Noire (French Massif Central). *Journal of Metamorphic Geology* 34: 447–462.

Frey M. Very low grade metamorphism of clastic sedimentary rock. In: Frey M, ed. *Low temperature metamorphism*. New York: Chapman and Hall, 1987, pp. 9–58.

Frey M, Robinson D. (eds) 1999. Low-grade metamorphism. Blackwell, 313 p.

Fukuchi R, Fujimoto K, Kameda J, Hamahashi M, Yamaguchi A, Kimura G, *et al.* 2014. Changes in illite crystallinity within an ancient tectonic boundary thrust caused by thermal, mechanical, and hydrothermal effects: an example from the Nobeoka Thrust, southwest Japan. *Earth, Planets and Space* 116: 1–12.

García-López S, Bastida F, Aller J, Sanz-López J. 2001. Geothermal palaeogradients and metamorphic zonation from the conodont colour alteration index (CAI). *Terra Nova* 13(2): 79–83.

Gerya T, Stöckhert B. 2002. Exhumation rates of high-pressure metamorphic rocks in subduction channels: The effect of Rheology. *Geophysical Research Letters* 29: 1261–1264.

Gèze B. 1949. Etude géologique de la Montagne Noire et des Cévennes méridionales. *Soc.Géol. Fr. Mém.* 62: 1–125.

Guggenheim S, Bain DC, Bergaya F, Brigatti MF, Drits VA, Eberl DD, *et al.* 2002. Report of the Association Internationale pour l'Etude des Argiles (AIPEA) Nomenclature Committee for 2001: Order, disorder and crystallinity in phyllosilicates and the use of the "Crystallinity Index". *Clay Minerals* 37: 389–393.

Guiraud M, Sauniac S, Burg JP. 1981. Précision sur les conditions Pression-Température lors de la mise en place de la nappe de Pardailhan (Montagne Noire), par la détermination des inclusions fluides. *Comptes-rendus de l'Académie des Sciences, Série II* 292: 229–232.

Hamet J, Allègre CJ. 1976. Hercynian orogeny in the Montagne Noire (France): Application of Rb87-Sr87 systematics. *Geological Society of America Bulletin* 87: 1429–1442.

Hara H, Kurihara T, Mori H. 2013. Tectono-stratigraphy and low-grade metamorphism of Late Permian and Early Jurassic accretionary complexes within the Kurosegawa belt, Southwest Japan: Implications for mechanisms of crustal displacement within active continental margin. *Tectonophysics* 592: 80–93.

Harris LB, Burg JP, Sauniac S. 1983. Strain distribution within the Pardailhan nappe (Montagne Noire, France), and structure of its basal thrust zone: implications for events associated with nappe emplacement. *J. Struct. Geol.* 5: 431–440.

Hilchie LJ, Jamieson RA. 2014. Graphite thermometry in a low-pressure contact aureole, Halifax, Nova Scotia. *Lithos* 208: 21–33.

Kouketsu Y, Mizukami T, Mori H, Endo S, Aoya M, Hara H, *et al.* 2014. A new approach to develop the Raman carbonaceous material geothermometer for low-grade metamorphism using peak width. *Island Arc* 23: 33–50.

Kretschmer S, Franke W, Wemmer K, Köngigshof P, Gerdes A. 2015. Tectono-metamorphic evolution of the Mouthoumet Massif (Variscides, S-France): Interference of orogenic accretion and crustal extension. *Géologie de la France* 1: 78.

Kübler B. 1964. Les argiles, indicateurs de métamorphisme. *Revue Institut de la Française de Pétrole* 19: 1093–1112.

Kübler B. 1968. Evaluation quantitative du metamorphism par la cristallinite de l'Illite. *Bull. Centre Rech. Pau-SNPA* 2: 385–397.

Lahfid A, Beyssac O, Deville E, Negro F, Chopin C, Goffé B. 2010. Evolution of the Raman spectrum of carbonaceous material in low-grade metasediments of the Glarus Alps (Switzerland). *Terra Nova* 22: 354–360.

Le Bayon R, Brey GP, Ernst WG, Mählmann RF. 2011. Experimental kinetic study of organic matter maturation: time and pressure effects on vitrinite reflectance at 400 °C. *Organic Geochemistry* 42: 340–355.

Lescuyer JL, Bouchot V, Cassard D, Feybesse JL, Marcoux E, Moine B, *et al.* 1973. Le gisement aurifère de Salsigne (Aude, France) : une concentration syntectonique tardivarisque dans les sédiments détritiques et carbonatés de la Montagne Noire. *Chronique de la Recherche Minière* 512: 3–73.

Mählmann RF. 2001. Correlation of very low-grade data to calibrate a thermal maturity model in a nappe tectonic setting, a case study from the Alps. *Tectonophysics* 334: 1–33.

Mählmann RF, Bozkaya Ö, Potel S, Le Bayon R, Šegvić B, Nieto F. 2012. The pioneer work of Bernard Kübler and Martin Frey in very low-grade metamorphic terranes: paleo-geothermal potential of variation in Kübler-Index/organic matter reflectance correlations. A review. *Swiss Journal of Geosciences* 105(2): 121–152.

Malavieille J. 2010. Impact of erosion, sedimentation and structural heritage on the structure and kinematics of orogenic wedges: analog models and case studies. *GSA Today* 20: 4–10.

Mattauer M, Laurent P, Matte P. 1996. Plissement hercynien synschisteux post-nappe et étirement subhorizontal dans le versant sud de la Montagne noire (Sud du Massif central, France). *Comptes rendus de l'Acad. des Sciences, Série 2* 322: 309–315.

Matte P, Lancelot J, Mattauer M. 1998. La zone axiale hercynienne de la Montagne Noire n'est pas un "metamorphic core complex" extensif mais un anticlinal post-nappe à cœur anatectique. *Geodinamica Acta* 11: 13–22.

Merriman R, Frey M. Patterns of very low-grade metamorphism in metapelitic rocks. In: Robinson D, Frey M, eds. *Low-grade metamorphism*, 1999, pp. 61–108.

Merriman R, Peacor DR. Very low-grade metapelites: mineralogy, microfabrics and measuring reaction progress. In: Robinson D, Frey M, eds. *Low-grade metamorphism*, 1999, pp. 10–60.

Mori H, Wallis S, Fujimoto K, Shigematsu N. 2015. Recognition of shear heating on a long-lived major fault using Raman carbonaceous material thermometry: implications for strength and displacement history of the MTL, SW Japan. *Island Arc* 24: 425–446.

Mori H, Mori N, Wallis S, Westaway R, Annen C. 2017. The importance of heating duration for Raman CM thermometry: evidence from contact metamorphism around the Great Whin Sill intrusion, UK. *Journal of Metamorphic Geology* 35: 165–180.

Mukoyoshi H, Hirono T, Hara H, Sekine K, Tsuchiya N, Sakaguchi A, *et al.* 2009. Style of fluid flow and deformation in and around an ancient out-of-sequence thrust: An example from the Nobeoka Tectonic Line in the Shimanto accretionary complex, southwest Japan. *Island Arc* 18: 333–351.

Mullis J, Mählmann RF, Wolf M. 2017. Fluid inclusion microthermometry to calibrate vitrinite reflectance (between 50 and 270 °C), illite Kübler-Index data and the diagenesis/anchizone boundary in the external part of the Central Alps. *Applied Clay Science* 143: 307–319.

Pitra P, Poujol M, Van Den Driessche J, Poilvet JC, Paquette JL. 2012. Early Permian extensional shearing of an ordovician granite: The saint-eutrope "c/s-like" orthogneiss (montagne noire, French massif central). *Comptes Rendus Géoscience* 344(8): 377–384.

Poilvet JC, Poujol M, Pitra P, Van Den Driessche J, Paquette JL. 2011. The Montalet granite, Montagne Noire, France: An Early Permian syn-extensional pluton as evidenced by new U-Th-Pb data on zircon and monazite. *Comptes Rendus Géoscience* 343(7): 454–461.

Poty É, Aretz M, Barchy L. 2002. Stratigraphie et sédimentologie des « calcaires à Productus » du Carbonifère inférieur de la Montagne noire (Massif central, France). *Comptes Rendus Geoscience* 334: 843–848.

Rahl JM, Anderson KM, Brandon MT, Fassoulas C. 2005. Raman spectroscopic carbonaceous material thermometry of low-grade metamorphic rocks: calibration and application to tectonic exhumation in Crete, Greece. *Earth and Planetary Science Letters* 240: 339–354.

Rahn M, Mullis J, Erdelbrock K, Frey M. 1995. Alpine metamorphism in the north Helvetic flysch of the Glarus-Alps, Switzerland. *Eclogae Geologicae Helvetiae* 88: 157–178.

Roger F, Respaut JP, Brunel M, Matte P, Paquette JL. 2004. Première datation U-Pb des orthogneiss œillés de la zone axiale de la Montagne noire (Sud du Massif central): nouveaux témoins du magmatisme ordovicien dans la chaîne Varisque. *Comptes Rendus Geoscience* 336: 19–28.

Roger F, Teyssier C, Respaut JP, Rey PF, Jolivet M, Whitney DL, *et al.* 2015. Timing of formation and exhumation of the Montagne Noire double dome, French Massif Central. *Tectonophysics* 640: 53–69.

Sadezky A, Muckenhube H, Grothe H, Niessner R, Pöschl U. 2005. Raman microspectroscopy of soot and related carbonaceous materials: spectral analysis and structural information. *Carbon* 43: 1731–1742.

Sauniac S. 1980. Utilisation des exsudats de quartz come critères de reconnaissance d'un régime cisaillant: exemple de la base de la nappe de Pardailhan (versant sud de la Montagne Noire). *Rev. Géol. Dyn. Geog. Phys* 22: 177–186.

Schuiling R. 1960. Le dôme gneissique de l'Agoût (Tarn et Hérault). Mémoire de la Société Géologique de France, 91 p.

Soula JC, Debat P, Brusset S, Bessière G, Christophoul F, Déramond J. 2001. Thrust-related, diapiric, and extensional doming in a frontal orogenic wedge: example of the Montagne Noire, Southern French Hercynian Belt. *Journal of Structural Geology* 23: 1677–1699.

Thompson PH, Bard JP. 1982. Isograds and mineral assemblages in the eastern Axial Zone, Montagne Noire (France): implications for temperature gradients and P-T history. *Canadian Journal of Earth Sciences* 19: 129–143.

Trap P, Roger F, Cenki-Tok B, Paquette JL. 2017. Timing and duration of partial melting and magmatism in the Variscan Montagne Noire gneiss dome (French Massif Central). *International Journal of Earth Sciences* 106: 453–476.

Underwood M, Byrne T, Hibbard JP, DiTullio L. A comparison among organic and inorganic indicators of diagenesis and low-temperature metamorphism, Tertiary Shimanto Belt, Shikoku, Japan. In: Underwood M, ed. *Thermal Evolution of the Tertiary Shimanto Belt, Southwest Japan: An Example of Ridge-Trench Interaction*, 1993, pp. 45–61.

Vachard D, Aretz M. 2004. Biostratigraphical precisions on the Early Serpukhovian (Late Mississippian), by means of a carbonate algal microflora (cyanobacteria, algae and pseudo-algae) from La Serre (Montagne Noire, France). *Geobios* 37: 643–666.

Vachard D, Izart A, Cózar P. 2017. Mississippian (middle Tournaisian-late Serpukhovian) lithostratigraphic and tectonosedimentary units of the southeastern Montagne Noire (Hérault, France). *Géologie de la France* 1: 47–88

Van Den Driessche J, Brun JP. 1989. Un modèle cinématique de l'extension paléozoïque supérieur dans le Sud du Massif Central. *Comptes rendus de l'Académie des sciences. Série 2, Mécanique, Physique, Chimie, Sciences de l'univers, Sciences de la Terre* 309 (16): 1607–1613.

Van Den Driessche J, Brun JP. 1992. Tectonic evolution of the Montagne Noire (French Massif Central): a model of extensional gneiss dome. *Geodinamica Acta* 5: 85–97.

Velde B, Lanson B. 1993. Comparison of I/S transformation and maturity of organic matter at elevated temperatures. *Clays and Clay Minerals* 41: 178–178.

Vizcaïno D, Álvaro JJ. 2001. The Cambrian and lower Ordovician of the southern Montagne Noire: a synthesis for the beginning of the new century. *Ann. Soc. géol. Nord (2° sér.)* 8: 185–242.

Wada H, Tomita T, Matsuura K, Tuchi K, Ito M, Morikiyo T. 1994. Graphitization of carbonaceous matter during metamorphism with references to carbonate and pelitic rocks of contact and regional metamorphisms, Japan. *Contributions to Mineralogy and Petrology* 118: 217–228.

Weber K. 1972. Notes on the determination of illite crystallinity. *Neues Jahrbuch für Mineralogie, Monatshefte* 6: 267–276.

Whitney DL, Roger F, Teyssier C, Rey PF, Respaut JP. 2015. Syn-collapse eclogite metamorphism and exhumation of deep crust in a migmatite dome: the P-T-t record of the youngest Variscan eclogite

(Montagne Noire, French Massif Central). *Earth and Planetary Science Letters* 430: 224–234.

Wiederer U, Koenigshof P, Feist R, Franke W, Doublier MP. (2002). Low-grade metamorphism in the Montagne Noire (S-France): Conodont Alteration Index (CAI) in Palaeozoic carbonates and implications for the exhumation of a hot metamorphic core complex. *Schweizerische Mineralogische und Petrographische Mitteilungen* 82: 393–407.

Zhu C, Rao S, Hu S. 2016. Application of illite crystallinity for paleo-temperature reconstruction: A case study in the western Sichuan basin, SW China. *Carpathian Journal of Earth and Environmental Sciences* 11(2): 599–608.

Cite this article as: Montmartin C, Faure M, Raimbourg H. 2021. Paleotemperature investigation of the Variscan southern external domain: the case of the Montagne Noire (France), *BSGF - Earth Sciences Bulletin* 192: 3.